This is to certify that the
thesis entitled

THE PERSISTENCE OF GUNSHOT RESIDUE ON DECOMPOSING TISSUE

presented by

LUTHER STERLING SCHAEFFER

has been accepted towards fulfillment
of the requirements for the

MS degree in CRIMINAL JUSTICE

Major Professor's Signature

05/23/07

Date

The Persistence of Gunshot Residue on Decomposing Tissue

By

Luther Sterling Schaeffer

A THESIS

Submitted to
Michigan State University
In partial fulfillment of the requirements
for the degree of

MASTER OF SCIENCE

Criminal Justice

2007

ABSTRACT

The Persistence of Gunshot Residue on Decomposing Tissue

By

Luther Sterling Schaeffer

The research presented herein describes the development and optimization of scanning electron microscopy / energy-dispersive spectroscopy (SEM/EDS) and inductively-coupled plasma mass spectrometry (ICPMS) for the analysis of gunshot residue (GSR) on decomposing tissue. Two euthanized pigs were obtained from the MSU Swine Facility. One pig was shot 10 times with a Glock 9mm pistol and the other served as the source of the control tissue samples. Each day, a gunshot wound and a control tissue sample was excised from each pig over a 7-day sampling period. Three methods of sample preparation were attempted prior to SEM/EDS analysis; air-drying, freeze-drying, and tape-lifting. GSR consisting of Sb, Ba, and Pb was found by SEM and analyzed by EDS on the tape-lifts from days 1 and 2. ICPMS was used to analyze gunshot wounds and control tissue for ^{121}Sb, ^{138}Ba, and ^{208}Pb after preparing the samples by microwave digestion. GSR was determined in the gunshot wounds throughout the course of the 7-day sampling period in concentrations ranging from 9.19 μg of ^{121}Sb per gram of tissue (μg/g) to 0.15 μg/g, ^{138}Ba was determined in the range of 30.67 – 0.06 μg/g, and ^{208}Pb was determined in he range of 26.71 – 0.10 μg/g. ICPMS had a linear response between 0 – 1000 ppb for ^{121}Sb, ^{138}Ba, ^{208}Pb and the limits of detection were 0.002, 0.033, and 0.009 ppb, respectively.

ACKNOWLEDGEMENTS

First and foremost, I owe a great bit of gratitude to everyone who had contributed to this project.

Dr. Ruth Waddell, thanks for reading through this time and time again, you made it through all the tens of us racing theses for corrections. Thanks for all the guidance and suggestions on the project ranging from the research to the AAFS presentation and finally the written work.

Dave Szymanski (soon to be Dr.), thanks for all the help, guidance, and work for the ICPMS portion of this study, without your help this study would have been lacking.

Dr. Stanley Flegler, Carol Flegler, and everyone at the Center for Advanced Microscopy, you all have been invaluable resources throughout this work. Thank you for all your patience and passing on some of your knowledge to me.

Thanks also to Michael Blaskovitz, Dr. Brian Hunter, Dr. Rich Merritt, Dr. Norm Sauer, Al Snedegar, Mr. Firearms Specialist of Local PD.

Thanks to my family for once again enduring my frustrated diatribes. And finally thanks to all of my climbing friends for providing me with an essential outlet, support, and the opportunity to forget about my work.

Anyone who I may have left out, just because your name is not here does not mean you were forgotten, thank you.

TABLE OF CONTENTS

LIST OF TABLES

Chapter 3: Materials and Methods

Chapter 4: Results and Discussion

LIST OF FIGURES

Chapter 1: Introduction

Chapter 2: Instrumental Theory

Chapter 3: Materials and Methods

Chapter 4: Results and Discussion

Chapter 1

Introduction

1.1 Introduction

In 2005, the United States Department of Justice Bureau of Justice Statistics, reported that index crimes (rape, murder, robbery, aggravated assault, and property crimes) involving a firearm comprised about 68% of all murders, 42% of all robberies, and 21% of all aggravated assaults that were reported to the police nationally.[1] Approximately 30,000 deaths annually are a result of guns, and greater than 10,000 of those deaths are ruled homicide.[2] Of the 4.7 million violent crimes consisting of rape and sexual assault, robbery, and aggravated and simple assault that were reported in 2005, a total of 9% involved a firearm.

From the statistics given above, it is obvious that firearms related incidents are common occurrences in the US. Therefore it is of utmost importance for trauma specialists, medical examiners, and pathologists to be able to identify a gunshot wound when they are presented. Depending on the distance from which the gunshot wound was inflicted, the caliber of the firearm, and the state of bodily decomposition, the identification of a wound may not be a simple task due to reasons such as the lack of a discernable entrance wound, or in the case of decomposition, blackening of the skin. A study conducted by Collins et al. in 1994 revealed the difficulty trauma specialists face when attempting to distinguish the entrance from exit wound on mortally wounded bodies. The study reported that of 46 victims presenting gunshot wounds, 52% were misinterpreted

in terms of differentiating exit from entrance holes and identification of a gunshot wound.[3]

Physical examination of gunshot wounds can consist of many observations recorded by the consulted practitioner; the wound itself, fracturing of underlying bone, as well as gunshot residue (GSR) around the wound.[4] In a badly decomposed body, cause of death by gunshot wound may be difficult to discern if the wound itself is not visible and may be misidentified. In the absence of any other pertinent evidence, this can make cause of death determinations difficult for the forensic pathologist. In decomposed bodies where it is impossible to visually identify gunshot wounds, detection of GSR may allow for determination of the cause of death. Additionally, the examination of wounds for GSR may be of assistance to determine entrance from exit holes as well as the distance between firearm and target.[5]

1.2 Anatomy of a Cartridge

To understand GSR and its relevance to a forensic investigation it is imperative to first develop a general familiarity with firearms and ammunition. The lethality of firearms is derived from the ammunition cartridge. The cartridge unit is made up of four primary parts; the bullet, cartridge casing, propellant, and the primer, as seen in Figure 1.1. The bullet is securely housed in the cartridge casing, which is commonly made of brass and filled with a propellant. The propellant is a low explosive, either black powder or as is more commonly encountered, smokeless powder. Black powder is a mixture of potassium nitrate,

charcoal and sulfur in an approximate 15:3:2 ratio. Smokeless powder is made from nitrocellulose (single-base) or mixtures of nitrocellulose and nitroglycerine (double-base) or the previous two in addition to nitroguanidine (triple-base). Smokeless powders have a greater energy density than black powder and the combustion products are mainly gaseous, whereas black powder combustion produces approximately 33% solid products.[6] Bullets come in many different shapes, calibers, and are made from a variety of materials. Bullets are most often made from lead and may be covered in a layer of copper plating called a jacket. The jacket can partially cover the bullet, called a semi-jacketed bullet, or fully encapsulate it, termed a full metal-jacketed bullet.

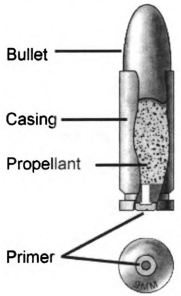

Figure 1.1. A cut-away diagram of a typical firearm ammunition cartridge revealing its basic components.

The primer is a small, compact explosive charge, which is packed into a primer cup at the base of the cartridge casing. The primer consists of 4

components; an initiating explosive, oxidizing agent, fuel, and sensitizer. The initiator is typically lead styphnate, the oxidizing agent is typically barium nitrate however barium peroxide, lead nitrate, or lead peroxide may also be used. The fuel is most commonly antimony sulfide, and the sensitizing agent often is tetracene.[7] When the primer is struck by the firing pin, the primer detonates which then ignites the propellant. The ignited propellant deflagrates into a rapidly expanding gas, which accelerates the bullet out of the cartridge casing and down the barrel of the gun. Spiraled grooves in the barrel of the firearm, termed rifling, cause the bullet to spin as it is propelled from the firearm. Rifling provides the bullet gyroscopic stability resulting in a straighter trajectory and maximum velocity on leaving the barrel.

1.3 Gunshot Residue (GSR)

Gunshot residue consists of a gaseous mixture of combustion products from the primer and propellant, as well as particulates from the bullet, cartridge casing, and the barrel of the firearm. The gaseous GSR is expelled from the barrel of the firearm along with the bullet, as shown in Figure 1.2.[7-9] GSR deposits on nearby objects such as the target as well as the shooters hands and clothes.

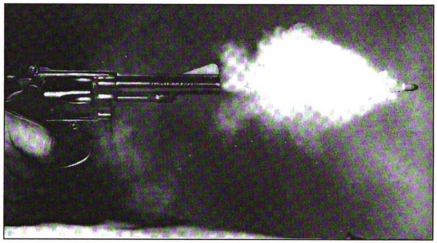

Figure 1.2. A handgun firing a bullet. The white cloud trailing the bullet is the plume of GSR.[10]

Expulsion of GSR causes a visible blackened circle of GSR to deposit on objects close to the end of the firearm barrel. At greater distances, the ring becomes more difficult to distinguish and larger in diameter as it becomes more diffuse.[11] A characteristic of GSR deposition, called stippling, is a pattern resulting from unburnt and partially burnt gunpowder embedding in the target. The mass of the gunpowder particles is greater than that of the smoke particulates and thus will travel further to distances of approximately 3 through 5 feet. GSR can be observed by the naked eye from firearms discharged at distances less than 12 inches from their respective target. At distances greater than 12 inches, it becomes much more difficult to discern GSR without the aid of staining or a microscope.[12]

GSR, as mentioned above, consists of trace materials derived from the primer, propellant, cartridge casing and the bullet itself. It has also been found to contain distinguishable trace elements from the cast material of the barrel of the

firearm.[13] The components of GSR which are considered characteristic for identification are derived from the primer of the cartridges, which contains compounds of barium (Ba), lead (Pb), and antimony (Sb). These materials combust and form the basis for the characteristic elemental profile of GSR; elemental Pb and Sb and compounds of Ba.[7] GSR also contains organic components from the propellant and primer; however, these are usually analyzed as supportive evidence when determined along with Ba, Pb, and Sb and will not be discussed any further in this text.[7]

Another characteristic beyond the elemental profile used for concluding the presence of GSR is the morphology of the particulates. GSR coalesces while in the gaseous state to form small spherical droplets in the range of 0.1 μM to 10 μM. Although larger sizes are occasionally seen, GSR is most commonly found in the latter size range.[8, 9] The particle morphology in conjunction with the elemental composition provides a distinct profile for GSR versus various other environmental or occupational contaminants such as automobile brake particles and exhaust particles as well as lead aerosols.[14, 15] Torre et al. showed that although analysis of individual particles of automobile brakes revealed an elemental profile consistent with GSR particles, the individual particles could be discriminated because they lacked the spherical morphology characteristic of GSR.[15] The studies by Torre and Wolmer illustrate the power of scanning electron microscopy/energy-dispersive spectroscopy (SEM/EDS) to analyze individual GSR particles and discriminate non-GSR particles of similar elemental profiles based on morphology.[15]

1.4 Methods of Elemental GSR Analysis

Many analytical methods and instrumental techniques have been described over the last 30 years for GSR detection[7, 8, 16] including: neutron activation analysis (NAA), capillary electrophoresis (CE), flameless atomic absorption spectroscopy (FAAS), SEM/EDS, and recently, inductively-coupled plasma mass spectrometry (ICPMS).[5, 17-24] The methods will be briefly discussed below, however, the reader is referred to one of several recent review articles in publication for additional details.[7, 8, 16]

Ruch et al. first documented analysis of GSR by NAA in 1964.[25] NAA provided a sensitive means to analyze GSR from shooters hands and clothing for Ba and Sb, but not Pb. The method was used for over a decade but suffered from major drawbacks such as requiring access to a nuclear reactor and specially trained individuals to perform the analysis.[8] Application of FAAS for GSR analysis followed in the early 1970s boasting the capability for sensitive analysis of Sb, Ba, and Pb.[7] Koons et al. reevaluated methods for GSR extraction followed by detection by FAAS. GSR was collected by scrubbing shooters hands with swabs moistened with 5% nitric acid and subsequent analysis was performed after extracting the sample from the cotton.[26] FAAS is a method possessing adequate sensitivity, however it lacks simultaneous multi-elemental analysis. Another method for simultaneous inorganic (Sb, Ba, and Pb) and organic components of GSR by CE was introduced.[17] The method utilized cotton swabbing as described previously for sample collection. The CE method

was found to lack adequate sensitivity for real samples and would require sample preconcentration or large sample injections.[17]

The most widely used and accepted method of GSR analysis is SEM/EDS due to its ability to differentiate individual GSR particles by their morphology as well as their elemental composition.[16, 17, 27] Morphological and elemental analysis allows for the discrimination of particles, which may have the same elemental profile but clearly are not morphologically characteristic of GSR.[15] The large drawback of SEM/EDS analysis of GSR is it is a cumbersome method; it can take several hours to perform elemental and morphological analysis. Advancement of this method include programs that automate the procedure of particle analysis and low vacuum systems which require very little sample pretreatment.[16, 27-30]

A survey of crime labs conducted by Singer et al. revealed that bulk analysis of elemental GSR is most often performed by FAAS.[16] Recent publications, however, describe another alternative, ICPMS, as a promising method for trace elemental analysis.[5, 31] Benefits of ICPMS are its low detection limits, rapid-analysis time, isotopic analysis, wide linear dynamic range, and multi-elemental analysis capabilities.

1.5 Research Objectives

Numerous papers have been published in which the detection of GSR has been conducted from materials such as hand swabs, tape lifts, and clothing materials, however there is a very limited assortment of papers which address

GSR determined from biological tissues. The primary objective of this research is to evaluate the applicability of SEM/EDS and ICPMS for the detection of GSR located directly on decomposing tissue since the use of either of these techniques may be a useful tool for identifying gunshot wounds on bodies in advanced stages of decay. The details of appropriate tissue sample collection methods and storage procedures, as well as sample preparation and instrumental analysis procedures will be discussed.

Chapter 2

Instrumental Theory

2.1 Scanning Electron Microscopy / Energy Dispersive Spectroscopy (SEM/EDS)

The credit for building the first functional scanning electron beam microscope is given to Manfred von Ardenne.[32] Vast improvements of the design and functionality of the SEM followed over the course of the next 15 years by researchers such as Vladimir Zworykin, James Hillier, Gerald Snyder, and Sir Charles Oatley.[32, 33] Cambridge Instruments introduced the first commercially produced model in 1964. Since its commercial production, there have been many more developments for electron microscopy, including x-ray microanalysis for elemental identification.[33]

Compared to the light microscope, SEM provides an analyst not only with a superior resolution and magnification, but also the ability to identify elemental metal composition of samples when equipped with an x-ray analyzer. SEMs are continually being applied to new applications in failure analysis and in pathology, forensic, geological, metallurgical, and environmental labs.[28] There are an estimated 50,000 operating SEMs worldwide.[32] The SEM has the ability to image samples down to 3 nanometers with magnifications up to 300,000x making it very attractive to demanding detail oriented analyses like those commonly encountered in forensic trace analysis.[28] Forensic applications

include identification of diatoms, fiber and hair analysis, and trace material analysis, such as GSR.

A basic SEM design is illustrated below in Figure 2.1. The SEM consists of many components that need to be in perfect working order in order to generate a high quality image. The first essential step of successful imaging via electron microscopy is the production of an electron beam, which requires that the entire system be under high-vacuum (in the order of $<10^{-9}$ atm). The electron beam is generated by an electron gun located at the top of the SEM column in the electron gun chamber. The electron gun is typically one of three types; tungsten-hairpin filament, lanthanum-hexaboride crystal, or field-emission.[33]

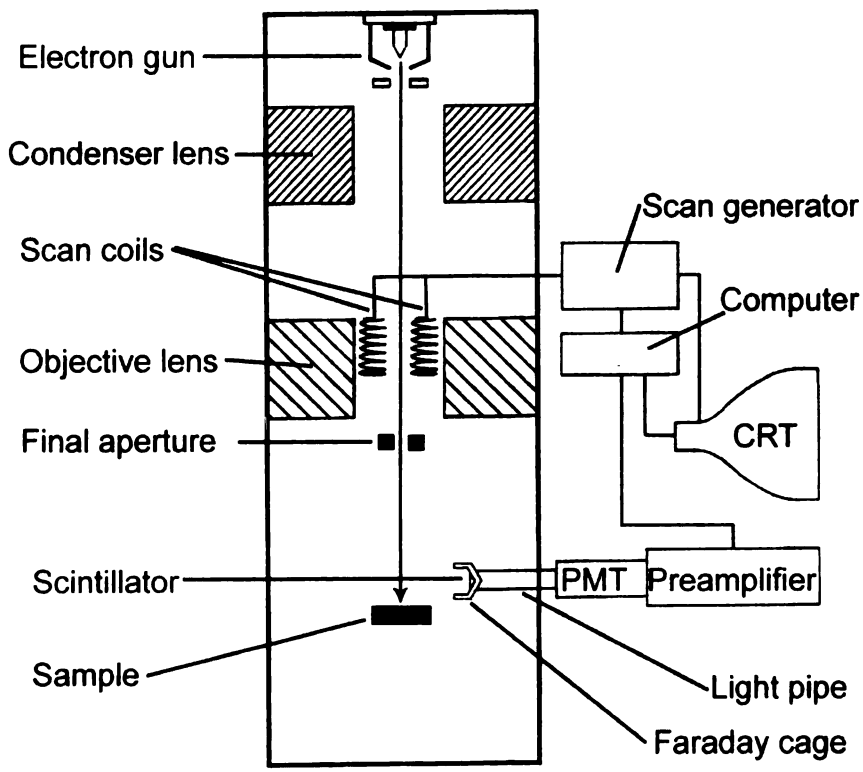

Figure 2.1 Block diagram of a scanning electron microscope. PMT – photomultiplier tube, CRT – cathode ray tube. Illustration was adapted from Flegler et. al.[33]

The tungsten filament emitter is the most cost-effective electron gun and does not require an ultrahigh vacuum, however it has a relatively short lifetime and it is not a strong emitter. The lanthanum-hexaboride (LaB_6) electron gun produces a much stronger electron beam under similar conditions, provides a superior resolution, and has a lifetime ten times that of the tungsten filament. The LaB_6 emitter however requires a higher vacuum and is much more expensive to replace. The third choice is the field-emission emitter, which produces an electron beam intensity up to 1000 times that of the tungsten filament with a resolution better than both of the former choices and a lifetime around 100 times that of the tungsten. Disadvantages of this emitter are its high cost, the need for a specially designed SEM, and an even higher vacuum than the LaB_6 emitter. More importantly, the field-emission emitter does not provide a stable electron beam.[33]

The electron beam travels from the gun through an anode aperture, limiting the beam size and eliminating stray electrons, and into focusing electromagnetic lenses. The electromagnetic lenses serve as a means to condense and focus the electron beam into the desired spot size. Focusing of the beam is performed by changing the amount of current applied to the lenses via a microscope control. Two types of lenses are used in the SEM; condenser and objective lenses. The condenser lens forces the initial electron beam into a smaller diameter. The objective lens then focuses the beam to a fine spot size. Within the objective lens, there are scan coils that are connected to a scan

generator. The scan coils create a varying electromagnetic field to move the focused electron beam back and forth over the sample in the form of scan lines.

When the electron beam strikes the sample, a complex series of interactions occur. These interactions of the electron beam and the sample atom electrons and nuclei result in the formation of variable energy electrons, x-rays, heat, and light. The low energy electrons resulting from inelastic collisions are ejected from the sample, these are termed secondary electrons (SE) and are used for imaging of the sample. The detector for SEM images is called an Everhart-Thornley detector. It consists of a Faraday cage with a positive bias of +300 V in order to attract the SE. The collected SEs are then accelerated by a +12,000 V bias applied to the scintillator. The scintillator is typically a phosphor and Al coated disk that converts the SE into photons. Photons are transmitted through the light pipe to outside of the vacuum of the SEM column into a photomultiplier tube (PMT). The PMT amplifies the initial photon signal, which then enters a preamplifier before finally terminating as an image on the cathode-ray tube (CRT).

The elastic collisions of the electron beam with the sample forms another type of higher energy electrons, termed back-scattered electrons (BSE). BSE are high-energy electrons reflected backward from the same side they entered. Their high energy is enough to overcome the positive bias applied to the Faraday cage where they strike a BSE semiconductor detector. The detector is mounted on the final aperture and produces an image that has much less resolution than the SE image. Though the resolution of BSE images are generally poor, they do

provide important information. BSE images allow for one to differentiate elements of differing atomic number. These images do not however provide the actual atomic number, but merely relative approximations.[33] Elements of higher atomic number result in brighter contrast than lower atomic numbers.

X-rays are another result of the complex sample-beam interaction. The detection of X-rays is an important feature of SEM because they allow for the determination of the spatial distribution of elements within a sample. X-rays are photons resulting from inelastic scattering events. When an electron strikes the sample, it can result in the ejection of an electron from an inner orbital shell. An electron from a higher energy shell then fills the inner orbital vacancy. The energy difference between the two shells may be emitted in the form of an X-ray. The energy and the wavelength of the produced X-ray is characteristic of the element from which it originated.[33] X-rays are named according to the shell from which they originate (K, L, M, N) followed by a subscript denoting the number of shells the electron which filled the vacancy has jumped (1 = α, 2 = β).[33] Each element typically produces several different energies of X-rays due to the different, quantized transitions that can occur within the atom. Each type of electron is called a line; the generation of enough X-rays of a particular line results in a peak corresponding to the energy of the X-ray, which is characteristic of the element that produced it.[33]

The X-ray detector attached to the SEM column can be one of two types, either wavelength-dispersive (WDS) or energy-dispersive (EDS) spectroscopes. EDS, the detector on the SEM used throughout this research, has several distinct

advantages over WDS. A full elemental analysis can be performed with EDS simultaneously, whereas with WDS a maximum of 4 selected elements can be analyzed at one time. The cost of the EDS system is also approximately one quarter of the WDS system. EDS is also beneficial for biological samples due to its greater sensitivity at low beam currents. WDS however has a greater selectivity than EDS allowing for 10x the ability to differentiate elements with similar spectra.[33]

The EDS system is made up of two main components: the detector and the analyzer. The detector consists of a solid-state crystal and a thin beryllium window that is protected by a collimator. The collimator is a housing column that protects the detector from stray X-rays and BSE. The window isolates the detector crystal from contaminants in the SEM column. The detector crystal is a lithium-doped silicon wafer semiconductor which converts the incident X-rays into a brief voltage pulse. The detector apparatus is kept cooled by liquid nitrogen to maintain the semiconductor properties of the detector crystal intact, to prevent the crystal from shorting out, and to eliminate electronic noise. The analyzer for the EDS system amplifies the voltage pulses of the X-rays, converts the analog signal into a digital form, and then sorts the digital pulses into channels so that a computer can then display the resultant spectra. The spectra consist of a plot of X-ray intensity (counts) versus X-ray energy.

2.2 Analysis of GSR Using SEM/EDS

Analysis of GSR by SEM/EDS is recognized as a selective and definitive method of analysis. SEM/EDS allows an investigator a great deal of specificity to image and determine morphological and elemental profiles of individual GSR particles compared to bulk methods of analysis such as atomic absorption spectroscopy and neutron activation analysis briefly described in Chapter 1.[10, 16, 34] The method has been recognized as a invaluable tool for GSR analysis since it was first demonstrated by Boehm in 1971.[35] Since its initial introduction, many researchers have described various methods of SEM/EDS analysis for GSR. The basic instrumental technique remains consistent with minor changes in the areas of sample preparation and sampling. A great deal of research focuses not necessarily on optimizing detection conditions but on the sample collection procedure.[22, 27]

The most commonly encountered GSR preparation method is via tape lift where a double-sided adhesive is mounted on an aluminum stub and then used to dab the sample.[10, 22, 36] The aluminum stub is the platform on which specimen analyzed by SEM are mounted. Using a tape lift has several distinct advantages such as sample stability with respect to time since the tape does not degrade as tissue does, simplicity of preparation, minimization of interferences such as epidermal cells in biological tissues, and a homogenous background signal contribution. The tape lift method is reported as the most effective sample preparation approach compared with other lifting techniques such as the glue-lift and concentrating techniques.[22]

Sample requirements for SEM/EDS analysis dictate that a sample must be thoroughly dry and devoid of all volatile chemicals, mounted firmly on the sample stub, and electrically conductive. The presence of volatiles or water in the sample can contaminate the vacuum of the SEM and an improperly mounted specimen can move or fall off the aluminum stub during insertion of the sample into the vacuum tube. The GSR samples collected by tape lifting satisfy the first two criteria, and to make them electrically conductive, the samples are coated with a thin layer of carbon via a carbon coater. The thickness of the carbon layer is typically in the range of 30 – 40 nm.[22]

2.3 Inductively-Coupled Plasma Mass Spectrometry (ICPMS) Theory

ICPMS was first commercially introduced in the late 1980s and has been extensively reviewed by researchers for a diverse range of multielemental trace analysis applications.[37, 38] ICPMS can be used for analysis of solid and solution-phase samples, however, the focus of the writing contained herein will describe its use and fundamental working principles from the solution-phase stand-point. ICPMS remains a popular technique of elemental analysis because of its low detection limits, selectivity, wide linear-dynamic range, good precision and accuracy and its ability to perform rapid multielemental analyses.[39, 40]

The ICPMS instrument is composed of two main components: the inductively-coupled plasma (ICP) source and the mass spectrometer (MS). Sample ions are generated in the ICP and then accelerated into the MS for

separation by mass to charge ratio and subsequent detection. A diagram of an ICP torch can be seen in Figure 2.2.

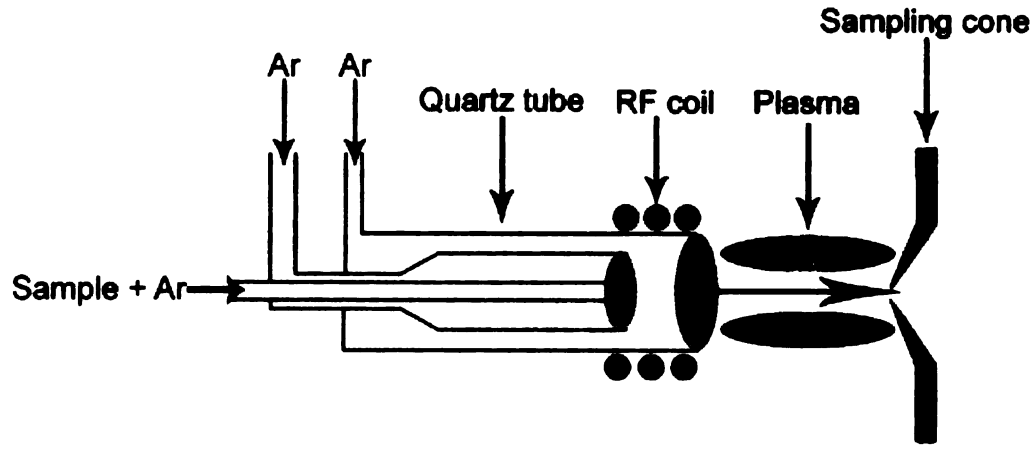

Figure 2.2 A schematic diagram of an ICP torch and its orientation with regards to the sampling cone of the MS.

The ICP is composed of a pneumatic sample nebulizer where a stream of argon (Ar) gas aerosolizes the injected solution-phase sample into a fine mist. The finer droplets are swept into the center channel of the plasma and heated to >8000 °C.[38] The torch consists of three annular tubes made from quartz, or another high-temperature resistant material, wrapped with an rf coil. The rf coil generates a high power radio frequency which inductively transfers the energy to the Ar, forming an electromagnetic field within the stream of gas. An electric spark is delivered to initiate the plasma which is then self-sustained at atmospheric pressure.[40, 41]

The tubes making up the torch carry Ar of different flow velocities through the rf coil region. Ar through the inner and secondary tubes is a support gas (0-1 L/min), which enters the rf coil region and is seeded with free energy from the

Tesla discharge coil. The electrons interact with the magnetic field and gain energy, which then ionizes Ar leading to a self-sustained plasma. The sample is then introduced in a flow of Ar through inner tube (~1 L/min). The outermost stream of Ar serves as a coolant with a high flow velocity (~15 L/min). The coolant stream dissipates heat generated by the torch and centers and stabilizes the plasma. The solution sample is introduced in a flow of Ar through the center quartz tube, typically at a lower flow rate (0.13-1.5 L/min).[41] As the sample aerosol passes through the hot core of the plasma, the sample is desolvated, dissociated into individual atoms, and ionized through the interaction with the plasma, all before entering the MS. The sample introduction efficiency is reportedly between 1 – 15% for ICP and more than two thirds of the elements on the periodic table are > 80% ionized in the torch.[41, 42]

Since the ICP is operated at atmospheric pressure and the MS must be operated under vacuum, the ionized sample must pass through a series of differentially pumped chambers of sequentially decreasing pressure before entering the MS.[38, 42] The sample ions enter the first vacuum chamber through a 1 mm hole in a nickel, water-cooled cone, called the sampling cone. The sampling cone is aligned axially with the ICP central channel to optimize ion transport into the MS. A slight vacuum is maintained behind the sampling cone (approximately 2 x 10^{-3} atm) and serves as the first chamber of sample introduction.[42]

Upon entry into the expansion chamber, the ionized sample and Ar expand rapidly due to the change in pressure and form a shock-wave structure

called a Mach disc.[42] A skimmer cone, much like the sampling cone protrudes into the Mach disc and has a centrally located hole of 0.7 mm diameter. The skimmer cone samples ions into an intermediate vacuum stage (< 10^{-7} atm) in the form of an ion beam. The ion beam is deflected along a narrow path via a series of electrostatic lenses into the mass analyzer.[42] Under the influence of the electrostatic lenses, positive ions are focused and separated from electrons and neutral particles.

The mass analyzer then separates the ions based on a mass-to-charge ratio (m/z). The quadrupole mass analyzer, like that used in this research, consists of four metal rods arranged to form a hyperbolic cross section. Controlled RF and direct current (DC) voltages are then applied to the rods which form an electric field within the area bounded by the rods and serve as an ion filter. Dependent on the RF/DC ratio, ions of a narrow m/z are able to pass through the m/z filter to the detector. All other m/z ions hit the rods, are neutralized and hence, are not detected. The ions that pass through the quadrupole mass analyzer then strike a dynode detector. The initial ion beam is converted into electrons for detection.[38, 42] By scanning the RF/DC ratio sequentially, ions of different m/z travel through the area bounded by the rods unhindered and reach the detector. Hence, a mass spectrum of the full mass range is obtained.

2.4 ICPMS for GSR Detection

Very few papers have discussed the analysis of GSR by ICPMS, possibly due to the high price of the instrument and lack of availability. However, ICPMS instrumentation is decreasing in price making this technique more accessible.[43] Although little has been published on this particular application, the instrument remains very popular for many other areas of trace elemental analysis such as geological and marine sciences.[37] At the time of this writing, five papers were located dealing specifically with GSR analysis by ICPMS, one from 1998, 2003, 2004, and two from 2007.[5, 31, 44-46] Three reports detailed collection of GSR from shooters hands through cotton swabs wetted with either 5% nitric acid or 2% solutions of ethylenediaminetetraacetic acid (EDTA).[44-46] The swabs were allowed to digest in a 10% nitric acid bath followed by sonication, dilution and analysis by solution-phase ICPMS. Koons reported the limits of detection for ^{121}Sb, ^{138}Ba and ^{208}Pb for his method involving 5% nitric acid were 0.05 μg/L, 0.02 μg/L and 0.1 μg/L, respectively, with relative standard deviations of <5% for all three elements.[44] Reis reported similar values for the 2% EDTA swabs of GSR, with detection limits of 0.05 μg/L, 0.51 μg/L, and 0.12 μg/L for ^{121}Sb, ^{138}Ba, and ^{208}Pb, respectively.[45] The third paper, a follow-up to Reis's work, used a similar sampling procedure to analyze GSR from two types of pistols using two different ammunition types with the 2% EDTA method.[46] In this paper, Sarkis did not report any novel observations or results.

Of the remaining two papers, one describes a method of extracting GSR from larvae removed after feeding on decomposing beef into which 2 shots had

been fired.[31] Roeterdink described a method of digesting larvae in concentrated nitric acid on a hot plate, with several steps of drying and reconstituting the sample before ICPMS analysis. The study detected significantly higher levels of ^{121}Sb, ^{138}Ba, and ^{208}Pb in larvae feeding on beef that was shot than control portions.

Santos and coworkers estimated firing distance based on ICPMS of bullet entrance holes.[5] The researchers fired onto cotton tissue paper at varying distances and cut 1 cm^2 squares from the targets at four radial distances from the gunshot hole. The squares were then digested for 24 hours in 10% nitric acid, sonicated, centrifuged, diluted, and then analyzed by ICPMS. The team determined that ICPMS was applicable for detecting GSR fired from distances as far as 80 cm and radial distances up to 5.5 cm from the bullet entrance hole. However, missing from the literature are studies that use ICPMS to detect GSR from tissue samples and decomposing tissue samples, which adds significance to the research reported herein.

Chapter 3

Materials and Methods

3.1 Experimental Design

Two euthanized pigs (200 lbs for GSR and 70 lbs for control) were obtained from the Michigan State University (MSU) Swine Facility. The animal use in this study was granted exemption from the guidelines set forth by the Michigan State University Institutional Animal Care and Use Committee (IACUC).

The larger pig was shot 10 times by a local firearms specialist using a Glock 9 mm with American Eagle 115 grain full-metal jacketed cartridges. Each shot was fired at a constant muzzle-to-target distance of 5 cm, spacing wounds at least 10 cm apart to minimize cross-contamination of gunshot residue between wounds (Figure 3.1). The gun was cleaned thoroughly between shots to prevent build-up of residue within the barrel. The pigs were then placed in a MSU research field and covered with a screen box to prevent attack by predators while still allowing exposure to weather.

Gunshot wounds were excised with a surgical scalpel from the shot pig daily for seven consecutive days. On day one, four wounds were excised from the shot pig; three wounds were used to optimize sample preparation and analysis procedures for both SEM/EDS and ICPMS, while the fourth wound was actually analyzed. On days two through seven, wounds were excised from the areas nearest the head first, working sequentially toward the rear of the pig. Previous studies conducted by the MSU forensic biology program indicated that

decomposition and larval destruction of the tissue occurred most rapidly at the head and progressed toward the rear of the carcass thereafter.

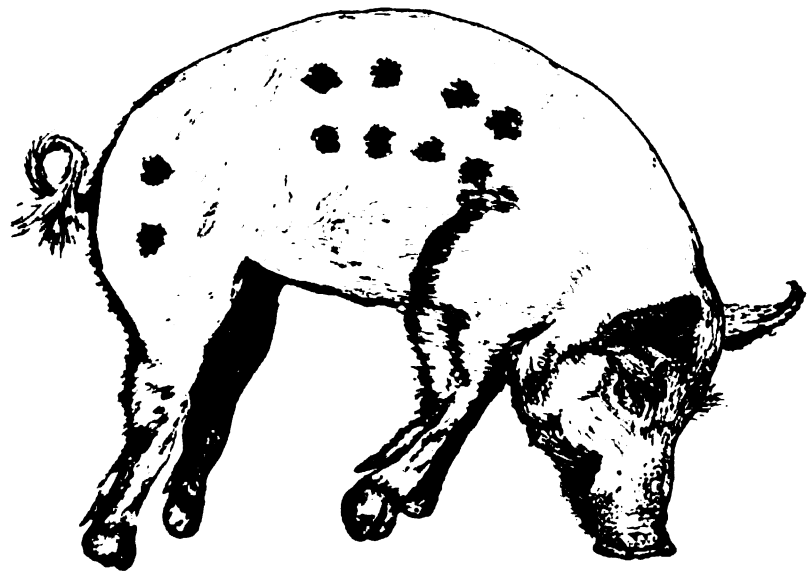

Figure 3.1 An illustration of the spacing and arrangement of the gunshot wounds on the pig. The illustration is not drawn to scale.

Hence, removing the wounds nearest to the head first ensured less potential for larval damage to the wound. Tissue samples were also excised from the control pig, one for each consecutive day. The tissue samples collected from the control pig were of approximately the same dimensions as the shot pig. The excised wound tissue was then wrapped loosely in wax paper and stored in a plastic bag in a freezer at -80 °C until analysis.

3.2 SEM/EDS Sample Preparation and Instrumental Parameters

Sample tissue for SEM/EDS was removed from the storage freezer and the adipose was removed. The sample was then prepared for analysis by either air-drying or freeze drying. The air-dried samples were stretched and pinned to a

small piece of cork board. The samples were elevated from the cork board by stretching the tissue over two disposable pipette barrels to prevent accumulation of moisture between the board and the tissue. The tissue was then placed in a glass petri dish and covered with a watch glass. The sample was allowed to dry for several days in a hood until it became translucent and rigid. The tissue was then removed from the cork backing and coated with a layer of carbon by a EFFA Carbon Coater (Ernest F. Fullam, Inc., Latham, NY).

Freeze-dried samples were inserted into a Flexi-Dry freeze-dryer (FTS Sytems, Stone Ridge, NY) held between the range of -54 °C and -84 °C and 25 mTorr for 24-48 hours until completely dried. The tissue was then coated in carbon as described previously. Both air-dried and freeze-dried samples were stored under vacuum in a dessicator until SEM/EDS analysis.

Tape lift of the gunshot wounds and control tissue was performed using small aluminum stubs with one face covered with double-sided adhesive carbon tape. The wounds were dabbed 100 times with the adhesive covered stub and then placed in a plastic Petri dish until analysis. The number of dabs used for sample collection was reported as the optimal amount in a review article which discussed the effectiveness of tape-lifting GSR versus number of dabbings.[16]

SEM analyses were conducted on a JEOL 6400V SEM (Japan Electron Optics Laboratories, Tokyo, Japan) equipped with a LaB_6 emitter and back-scattered electron detector. EDS analysis was completed with an INCAx-sight analyzer (Oxford Instruments, Oxfordshire, UK). EDS quantitative optimization was performed every 2 hrs through analysis of a pure copper grid affixed to the

brass sample housing. Dead-time was adjusted to lie within the range of 30-40%. The accelerating voltage was set to 20 kV and the working distance to 15 mm. Imaging was performed by both secondary and back-scattered electron detection.

3.3 ICPMS Sample Preparation

For ICPMS analysis of tissue, separate tissues were removed from the freezer, cut in half, and the adipose was removed from the skin using a clean surgical scalpel. One half of the tissue was used for ICPMS analysis, while the remaining portion was placed back into the freezer until analysis by SEM/EDS. The underlying flesh was discarded and the skin was used for analysis, as this research was concerned about the detection of GSR from decomposing tissue. Although there undoubtedly was some trace GSR in the bullet track, it was much less than that deposited topically around the wound. The skin from the control and wound tissue was then microwave digested.

Approximately 0.5 – 1.0 g of tissue was weighed out and placed in a 30 mL high-purity quartz vial (Milestone Inc., Shelton, CT). Along with the tissue inside the quartz vial, 2 mL of high-purity nitric acid (70%, Optima, Fisher, Pittsburgh, PA) and 1 mL of hydrogen peroxide were added. The quartz vial was then placed into a 100 mL Teflon-lined reaction vessel (Milestone Inc., Shelton, CT) that contained 10 mL deionized water and 2 mL of hydrogen peroxide. The reaction vessel was sealed to a uniform pressure using a calibrated torque wrench supplied with the digestion unit. The sample tissue was then digested

using a Milestone Ethos EZ microwave digestion system (Milestone Inc., Shelton, CT).

The digestion procedure started at ambient temperature followed by a 15 min. ramp to 200 °C at which the temperature was held constant for 10 min. before a final cool down back to ambient temperature. Temperature was digitally monitored via a thermo-coupled probe which was inserted into an enclosed thermowell located in one of the digestion vessels. The cool down was required to minimize the internal pressure of the reaction vessel. Typically, digestion vessels were opened once the internal temperature was below 100 °C. Of the digested tissue solution, 430 μL was then diluted to 2% nitric acid for ICPMS analysis. The remaining digest solution (approximately 2.6 mL) was stored under refrigeration at approximately 10 °C.

For the 7-day sampling period, one gunshot wound and control tissue sample was collected each day, resulting in a total of 14 tissues. The microwave digestion unit was able to digest 5 samples simultaneously, each batch consisted of 4 tissue samples and 1 blank in each batch. Along with each set of tissue samples that were digested, a procedural blank was run in order to evaluate any contamination. The procedural blanks were prepared by the above procedure except without any tissue samples. A procedural blank was run along with each batch of tissues digested, resulting in a total of 4 procedural blanks.

A cleaning step was performed to prevent cross-contamination between sets of digests. Cleaning was carried out by preparing the quartz vials and digestion vessels as described above except without any tissue samples. The

same microwave procedure was used as previously described and once the procedure was completed, the vessels were removed from the microwave, disassembled, and rinsed with deionized water. After the cleaning step, the next set of tissues were digested.

3.4 ICPMS Operating Parameters

Calibration standards and samples were analyzed on a Micromass (now Thermo Fisher Scientific Inc., Waltham, MA) Platform quadrupole ICPMS with a quartz torch (1.5 mm diameter injector), hexapole collision cell, and a CECTAC ASX-500 autosampler. Additional operational parameters are contained in Table 3.1 shown below. Tune conditions were optimized using a 10 μg/L solution of ^{9}Be, ^{59}Co, ^{115}In, ^{140}Ce, ^{209}Bi, and ^{238}U. Selected ion monitoring (SIM) was used for ^{138}Ba, ^{208}Pb, and ^{121}Sb with a sample scan time of 1.25 min. and a dwell time of 0.1 s.

Table 3.1 ICPMS instrumental parameters.

Parameter	Setting
Cool Gas Flow Rate	13.00 L/min
Auxiliary Gas Flow Rate	0.72 L/min
Sample Gas Flow Rate	0.72 L/min
RF Power	1350 W
Sampling Cone	Ni with Cu core, 1.14 mm diameter orifice
Skimmer Cone	Ni, 0.89 mm diameter orifice

Calibration standards of ^{138}Ba, ^{208}Pb, and ^{121}Sb were prepared in 2% nitric acid at concentrations of 0.5, 25, 250, 500, and 1000 μg/L by serial dilution. ^{115}In and ^{209}Bi were added as internal standards to the external standards, digested tissue, and procedural blanks. The calibration set was run at the beginning, half-way through, and at the end of tissue sample analyses to compensate for any ICPMS response drift or memory effects. Memory effects can be described as the retention of analytes within the system, which attribute to a greater response observed for subsequent sample injections.

Samples were injected via an autosampler and between each sample analysis, the injector was rinsed for 3 minutes with 2% nitric acid. The gunshot wound and control tissue digests as well as the procedural blanks were injected in the order of expected lowest analyte concentrations; the procedural blanks, followed by the control tissue samples, then the gunshot wounds starting with day 7, and proceeding through the highest expected analyte concentrations on day 1. This order was chosen in order to ensure that there would be minimal memory effects on the target analyte concentrations.

The instrument response for analytes in the samples was normalized to the internal standards. ^{115}In was used for normalization of ^{121}Sb and ^{138}Ba, and ^{209}Bi was used to normalize the response for ^{208}Pb in the tissue samples. The calibration curves were used for quantification of the concentration of analytes in the tissue samples. Concentrations determined by ICPMS were in parts per billion (ppb) which is equivalent to μg of analyte per liter of solution (μg/L). The

concentration was then multiplied by the dilution factor followed by the volume of solution in which the tissue was digested. The previous calculations determined μg of analyte in the stock digest, which was then divided by the sample tissue weight to result in μg element per gram of tissue (μg/g).

Chapter 4

Results and Discussion

4.1 Introduction

GSR has been studied a great deal over the course of several decades, however as revealed in the literature review in Chapter 2, there are very few papers discussing direct sample analysis.[16] In most reported analyses by SEM/EDS, GSR samples were collected by means of tape lifts.[7, 16, 19, 22, 27, 47] The researchers using bulk analytical methods such as FAAS and ICPMS mostly report that cotton swabs are first used to collect GSR from samples before analysis. The objective of this research was to determine the persistence of GSR in decomposing tissue, using SEM/EDS and ICPMS and analyzing the tissue directly rather than a swab of the tissue. In order to fulfill this objective, the project had three goals. First, the optimum method of sample preparation for SEM/EDS analysis of tissue samples containing GSR was determined and the applicability of SEM/EDS for direct tissue analysis was assessed. Second, ICPMS analysis of tissue samples containing GSR was investigated. Finally, the GSR content on decomposing tissue as a function of time, using both SEM/EDS and ICPMS, was investigated.

4.2 Decomposition Observations During Sampling Period

Porcine skin has been demonstrated to possess similar characteristics to human skin for gunshot residue studies as reported by Haag et al.[48] Hence,

tissue samples from pigs were used in this study to simulate human skin as closely as possible. Two pigs were used in the experiments discussed herein as a preliminary effort to lay the groundwork for future studies. Figure 4.1 is a picture of two gunshot wounds on the pig. Wounds had a noticeable blackened ring of soot and GSR with a radius of approximately 3 cm. Two black markings below the upper wounds show future wound sites, 10 cm apart.

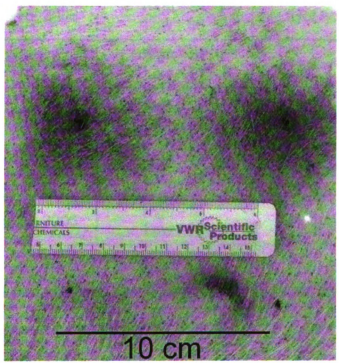

Figure 4.1 A picture of the resultant wounds and spacing on the pig.

After the pig was shot, both the control pig and the shot pig were transported from the firing range, placed about 2 meters apart in the MSU entomology field, and covered with separate screen boxes. The pigs were sampled daily during mid-July for a one-week period. The weather conditions, shown in Table 4.1, illustrate that during this particular week the Lansing area experienced a heat wave with high temperatures ranging from 87 – 96 ºF.

Table 4.1 The weather, dates, and temperature for the course of the seven day collection period.

Day	Date	Temperature (°F)	Weather
1	July 13, 2006	High - 87 Low - 64	Hot and sunny
2	July 14, 2006	High - 88 Low - 69	Sunny with p.m. rain showers
3	July 15, 2006	High - 91 Low - 68	Hot and sunny
4	July 16, 2006	High - 91 Low - 71	Hot and sunny
5	July 17, 2006	High - 92 Low - 67	Sunny until late afternoon, heavy p.m. rain
6	July 18, 2007	High - 86 Low - 63	Hot and sunny
7	July 19, 2006	High - 87 Low - 67	Hot and Sunny

During this period, it was sunny for the majority of the time, however there was a light rain shower over the night of the July 14th and torrential rain through the night of July 17th. Weather is of particular importance in this study because the elevated temperatures and rain cause decomposition to occur at an accelerated rate.[49, 50] The rain was of further concern because it was believed that it might wash away GSR making its detection by SEM/EDS and ICPMS difficult.

The pigs decomposed rapidly throughout the course of the week. On days one and two the shot and control pigs were becoming bloated and there was little insect activity (Figure 4.2a). The control pig was noticeably colonized

by insect larvae on the morning of day three and appeared to have similar larval activity as the shot pig. However, the progression of decomposition and desiccation that followed was much more rapid on the control pig than the shot pig.

The control animal was reduced to dried skin and bone by the 5th day; the larvae were much less active at this point and could be seen leaving the carcass. The difference in the speed of decomposition between the two animals may be due to the mass of the control pig versus the shot pig. The control carcass was about 70 lbs. compared to the shot pig, which was about 200 lbs. The larger pig accounted for much more tissue for insects to consume therefore taking a few days longer. For the shot pig, reduced larval activity was not observed until the 7th day, during which the larvae were observed migrating from the body. By day 8, the shot pig was reduced to a state (Figure 4.2b) comparable to that observed of the control pig on day 5.

a.)

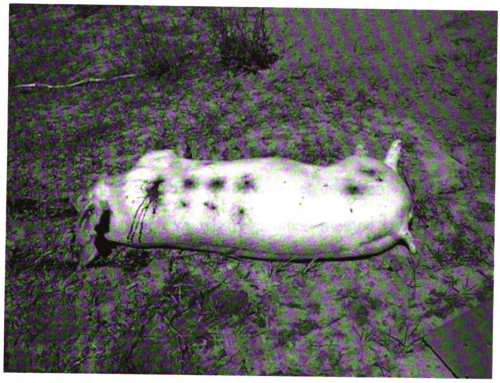

b.)

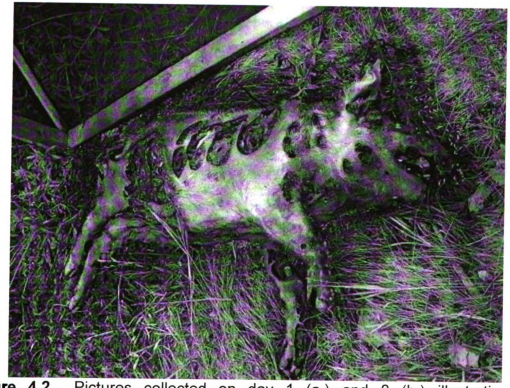

Figure 4.2 Pictures collected on day 1 (a.) and 8 (b.) illustrating the decomposition of the shot pig.

4.3 Analysis of tissue for GSR by SEM/EDS

4.3.1 Optimizing sample preparation for SEM/EDS analysis

Particular attention was paid to the method of sample preparation of wound tissue for SEM/EDS analysis of GSR. The methods of sample preparation had to leave the wound tissue relatively undisturbed for too harsh of a method would remove/dissolve GSR and ruin any chance of detection. For the previously stated reasons, a common sample preparation method for SEM, critical-point drying, could not be used. Critical-point drying requires that the sample be submerged in a series of solutions of increasing ethanol content to remove water before the final step of dehydration using liquid carbon dioxide.[33] The ethanol solutions would have removed GSR from the wound tissue.

Three methods of sample preparation were determined feasible and attempted; air-drying, freeze-drying and finally, tape-lifting GSR from the collected wound tissue.[16, 22, 33] For samples prepared by freeze-drying and air-drying, the adipose layer of the tissue was first removed with a clean surgical scalpel. Once the adipose was removed, samples that were air-dried were stretched and fixed to cork board. Samples took approximately four days until they were considered thoroughly dry, at which time the tissue was translucent and stiff. Samples that were freeze-dried were placed in the Flexi-Dry freeze dryer for 48 hours until the sample canister did not feel cold to the touch, as described in the Flexi-Dry manual. For tape-lifting, each tissue was dabbed 100 times with an adhesive-covered stub.

All samples analyzed by SEM/EDS were coated with a thin layer of carbon prior to analysis to ensure electrical conductivity. Without an adequate carbon layer, samples can become charged and appear bright white or appear dark, obscuring sample imaging and analysis. If the SEM images appeared either too bright at spots or too dark, the samples were promptly removed from the SEM chamber and coated with another layer of carbon.

Under the SEM, it was observed that the air-dried (AD) and freeze-dried (FD) tissues had very different features as illustrated in Figure 4.3. The AD tissue contracted to form a slightly ridged structure, whereas the FD tissue appeared more wrinkled. The AD sample images appeared much clearer than that of the FD sample as shown in the figures below. Despite the apparent clarity of the image, when the area to be searched for GSR was magnified, it became difficult to identify any GSR particles due to the debris and hair present on the surface of the tissue. At high magnification (~15,000x), the tissue was difficult to image without damaging the sample with the electron beam in the process.

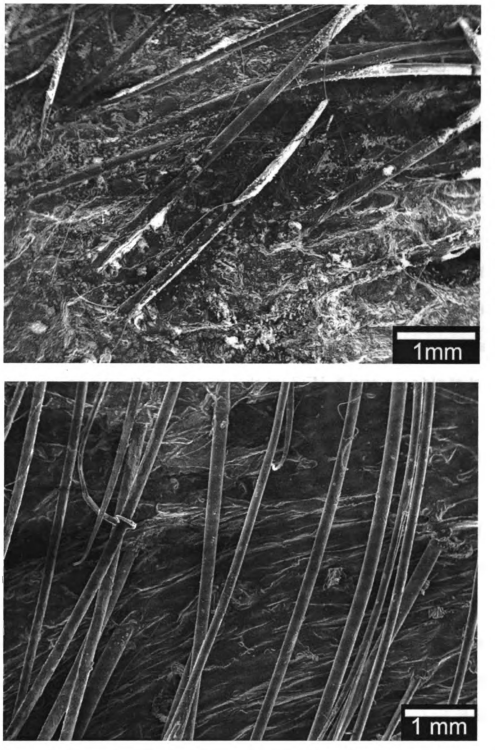

Figure 4.3 SEM images of freeze-dried (top) and air-dried (bottom) wound tissue prepared for analysis.

The FD samples appeared different from the AD sample; the FD sample had much more interfering debris and suffered from its greater sensitivity to the electron beam. FD samples, much like the AD tissue, had a greasy film coating them after preparation. At high magnifications and accelerating voltages, the FD samples could be observed to pucker and deform under the beam, more so than the AD sample. The SEM images that were collected lacked clarity and suffered still from poor electrical conductivity despite carbon coating.

All of the tissues directly analyzed by SEM, whether AD or FD, were difficult to image consistently. Samples from the control pig were also prepared via AD and FD and similar difficulties in sample preparation were encountered. Despite difficulties in viewing the AD and FD wounds by SEM, it was possible to locate GSR particles on wounds from days 1 and 2, as shown in Figure 4.4. The blurring at the bottom of the image is believed to be due to some latent moisture or other volatiles still present in the sample.

The GSR particles were located on the tissue by careful and tedious examination at high magnifications between 15,000 and 75,000x. Puckering of the tissue was observed at times from the electron beam interaction. The accelerating voltage was set to 25 kV in order to generate a detectable x-ray spectrum; this high energy is also sufficient to destroy the tissue. Imaging for too long a period on any one area led to the loss of focus of the image and at times the GSR particle would disappear from view. It is believed that the GSR particle would embed itself into the tissue when viewed at very high magnifications or

when imaged too long. Similar phenomena have been reported to happen on tape adhesive.[22]

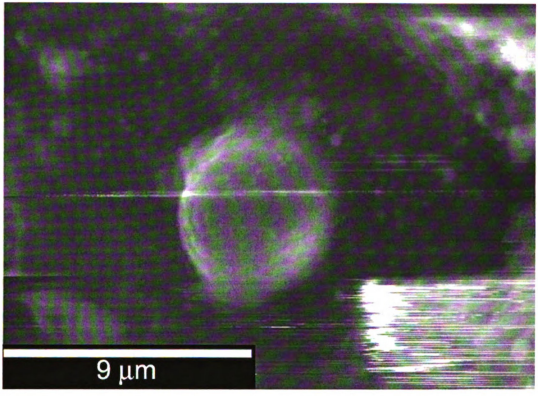

Figure 4.4 SEM secondary-electron image of a GSR particle from day 1 on an AD wound tissue sample.

Although the goal was to determine GSR directly on the tissue, it was apparent that direct analysis was much too difficult due to the changing surface of the tissue with time, the obscured GSR particles, and the labor-intensive sample preparation.

Tape-lifting provided a less labor-intensive approach for sample preparation as well as achieving consistent, clear images in which GSR was more easily located. Tape lifts of the gunshot wounds and control tissues were used for subsequent analyses due to the aforementioned reasons. Figure 4.5 has two

images; the first illustrates the clarity of the surface morphology of the carbon tape which was much more easily scanned for GSR than either the AD or FD tissues. The second image shows a back-scattered electron (BSE) capture of a tape-lifted sample of GSR from tissue collected on day 1.

The white dots in the bottom image in Figure 4.5 are images of GSR particles resulting from the electron interaction with the metals of the particulates. BSE detection is sensitive to increasing atomic number and the image produced shows differences in contrast proportional to atomic number; areas containing elements with higher atomic number appear brighter. This feature is related to the size of the atomic nucleus; a larger nucleus results in greater electron beam interaction and therefore more detectable signal is produced and detected. BSE images allow one to qualitatively differentiate GSR (higher atomic number) from the background (carbon tape).

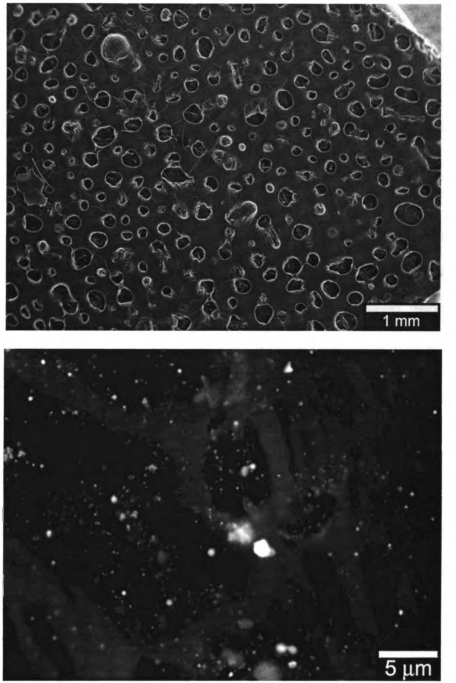

Figure 4.5 Images taken by SEM. A secondary electron image of unused carbon-coated carbon tape (top) and a back-scattered electron image of a tape-lift from a gunshot wound collected on day one (bottom).

4.3.2 SEM/EDS Analysis of Tape-lifts

The tape-lifts were taken for each of the gunshot wounds and corresponding control tissues (n = 14). The GSR was dense on tape lifts from wounds collected on days 1 and 2 and particles were easily located in under two minutes of searching. Example BSE and SE images are provided in Figure 4.6. The images illustrate the observable differences between the two detectors; BSE provides a high-contrast image capable of distinguishing differences in elemental atomic number, whereas the SE image provides a higher resolution image for observing morphological features. BSE imaging quickly revealed deposits of GSR at low magnification. GSR particles were then singled out and imaged at a much higher magnification until they took up most of the viewing screen.

The first feature that was observed was the size, shape, and morphology of the potential GSR particle. Several papers have described in detail the particle morphology encountered when analyzing GSR.[19, 27] The most common consensus is that GSR particulates are spherical in shape, some may be perfect spheres while others are irregular and distorted, which is most often the case observed in the research discussed herein.[19] The surfaces of the particles have been reported as being anywhere from smooth to resembling 'peeled oranges'.[27] The resolution of the particles imaged in this study was not adequate to definitively observe the topology of the particle surfaces. Most of the GSR particles that were detected throughout these analyses were in the 0.5 μm – 2 μm diameter size range and existed as individual spherical particles with a slight distortion on one side of the particle as seen in the images in Figure 4.6. Papers

have reported much larger particles in the area of 50 μm however, the largest that was discovered herein was approximately 9 μm.[27]

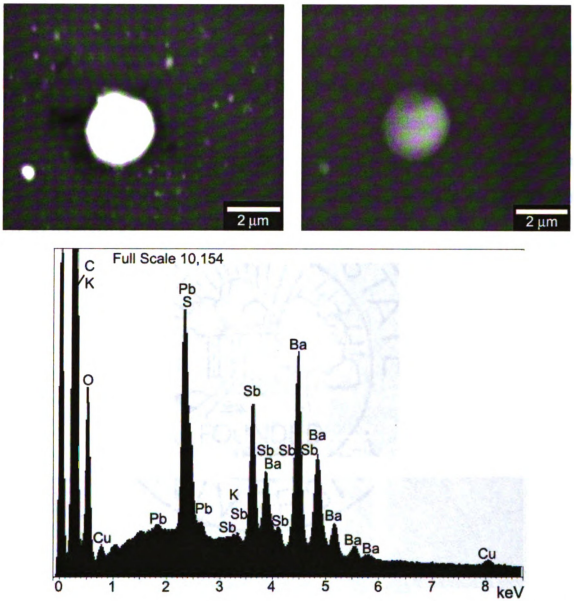

Figure 4.6 BSE (left) and SE (right) images for a single GSR particle on the tape-lift from a gunshot wound of day 1. The EDS spectrum below the images shows the elemental composition of the particle.

The elemental composition of a number of these particles was determined using EDS after initial imaging of the particle was performed. EDS analysis

indicated the presence of Sb, Ba, and Pb at detectable levels in most of the GSR particles located and analyzed. Figure 4.6 shows an x-ray spectrum resulting from the EDS analysis of the particle shown above in the same figure. As one can see, significant levels of Sb, Ba, and Pb were detected. The spectrum in Figure 4.6 reveals multiple peaks for each element as was discussed in Chapter 2. Elemental mapping (Figure 4.7) was also conducted and showed the distribution of each element detected by the analyzer. The mapping showed that the Sb, Ba, and Pb that was detected by EDS was actually within the particle and not the background.

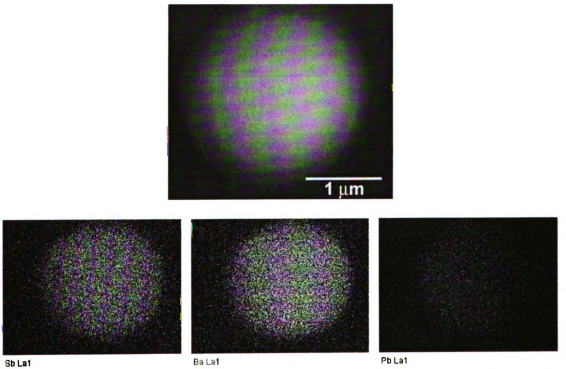

Figure 4.7 A SE electron image of a GSR particle from the tape lift of the gunshot wound from day 1 (above) and three elemental maps acquired by EDS detection showing the relative intensity of Sb, Ba, and Pb (L to R).

The combination of these three elements is considered a diagnostic criterion of GSR.[16, 27] Several studies have attempted to determine the elemental ratios of Sb, Ba, and Pb as well as other detected elements such as Cu and Al, but have concluded that each particle has large elemental variability.[19, 27] Each individual GSR particle may contain the same elements but not at the same levels.[16] In this study, the levels of Sb, Ba, and Pb were found to vary by several weight percent, as shown in Table 4.2 for the tape lifts of wounds from day 1.

Table 4.2 Average weight percent of Sb, Ba, and Pb in GSR particles collected from gunshot wound tissue sample of day 1.

	Weight %	**Standard Deviation (n = 8)**
Sb	1.44	0.83
Ba	2.60	1.99
Pb	12.60	9.87
Cu	0.34	0.17

As element abundances are highly variable, their presence is more diagnostic than the relative proportions of each. Due to such variation, it may not be possible to differentiate ammunition according to manufacturer based on elemental ratios. However, such differentiation may be possible based on trace elements present in the primer.[16, 51]

In the EDS spectra collected from the wounds on day 1 and 2, Cu was also routinely detected. The Cu that was detected was typically at much lower levels than the Sb, Ba, and Pb as shown in the x-ray spectrum in Figure 4.8. A

background spectrum of the carbon coated tape revealed the presence of trace Cu, which may contribute to the Cu observed in the sample spectrum. However, due to the levels of Cu observed in the sample, it is possible that the copper jacket of the bullet was also making a significant contribution to the elemental profile observed.

Aluminum was also observed in a few GSR samples, however, this element was observed very rarely. Figure 4.8 is an x-ray spectrum collected from one particular GSR particle located on the tape-lift of the gunshot wound tissue from day 2.

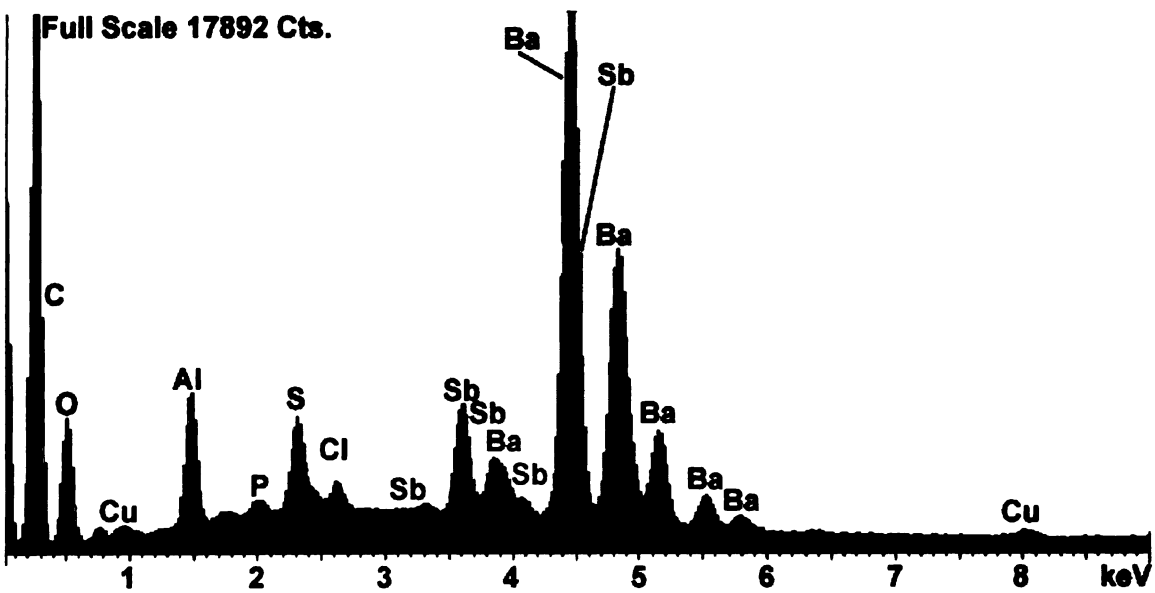

Figure 4.8 An x-ray spectrum for GSR located on the tape-lift from the gunshot wound sample collected on day 2. Of note is the aluminum peak in the spectrum.

According to the Federal Cartridge Company datasheet on the ammunition composition, Al is present in the 9 mm American Eagle cartridges which would explain its presence in the spectrum. The peak corresponds to 2.41

weight percent of the particle, which compared with the data in Table 4.2 falls between the average weight percents of Sb and Ba. No GSR particles containing Sb, Ba, and Pb were visible in wounds collected on days three through seven or on any of the control tissues. The fact that no GSR detected on control tissue indicates there was no contamination. However, the lack of GSR in wounds from days 3-7 was more surprising given the dense and easily visible GSR on day 2.

From Table 4.1, it can be seen that during the evening of day two, the area experienced a rainstorm. The rain may account for the abrupt loss of any detectable GSR on the following days. The GSR that was observed on days one and two consisted of very small particles, typically less than 1 μm in diameter and they were easily removed via tape-lift, leading to the conclusion that rain could have easily washed the loose GSR from the surface area around the wounds.

When analyzed by SEM, spherical particles were observed in the tape lifts from wounds collected on days 5 and 6. Initially, when imaged using BSE detection, these particles were thought to be GSR due to their bright appearance, indicating elements of high atomic number. However, analysis by EDS indicated that, while the spherical particles were in fact metal, the metal was a mix of Fe, Cr, and Ni (Figure 4.9) with no Sb, Ba, or Pb present. This combination of Fe-Cr-Ni is consistent with stainless steel alloys, which may be possibly derived from the barrel of the handgun. The particles detected on days five and six appeared different than the characteristic GSR found on days one and two. The Fe-Cr-Ni particles found on the day 5 and 6 gunshot wound tape lifts could be imaged with

better resolution than the GSR found on the tape lifts from the gunshot wounds of days 1 and 2. The Fe-Cr-Ni particles also appeared almost perfectly spherical whereas the GSR was spherical with slight deformation such as elongation.

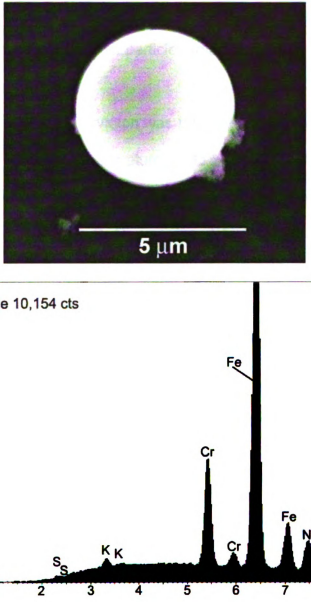

Figure 4.9 An example SEM image of the Fe-Cr-Ni metal particle discovered on a tape lift from day 5. The x-ray spectrum below shows the highest elemental abundance due to Fe.

The Fe-Cr-Ni particles have a similar morphology as D'Uffizi et al. described in their GSR research, however, the composition does not have any consistency with 'unique' GSR.[19] The Fe-Cr-Ni particles were also found to be slightly larger than the GSR with diameters between 3 – 5 μm. One paper briefly mentions the presence of Fe-Cr-Ni particles related to GSR but considers such particles of little evidential value.[27]

Another interesting observation was that the particles were found only on days five and six. Although no literature could be located which discusses this observation, it is supposed that it may be due to the physical properties of the particles themselves. The Fe-Cr-Ni particles were larger in diameter than the characteristic GSR that may have allowed for the particles to embed within the skin around the gunshot wound. As the tissue decomposed, the skin around the particles may have receded and exposed the Fe-Cr-Ni particles, which then on days five and six were easily tape-lifted from the wound. During the evening of day five, the area experienced heavy rain. Expectedly, the Fe-Cr-Ni particles would have been washed away as the GSR had been during the rain on the evening of day 2. However, on day five, six Fe-Cr-Ni particles were located and after the rain on day six, one was found, providing evidence that the Fe-Cr-Ni particles were more tightly bound than the GSR. On day seven no particles of GSR or Fe-Cr-Ni were located.

4.4 Summary of SEM/EDS Results

The results of this study are multidimensional. First and foremost, it was found that tape lifting GSR from tissue was more consistent and less labor-intensive than direct tissue analysis prepared either by air-drying or freeze-drying tissue samples. Tape lifts provided a more stable substrate for imaging the particles. With the tape lifts, high magnification and high accelerating voltages could be used in order to acquire clearer images and spectra whereas this was impossible on tissue since the substrate is so sensitive to the electron beam. It was also corroborated that elemental ratios for GSR were highly variable. The level of variability for each of the elements detected was large, indicating that elemental ratios may not be diagnostic for a cartridge manufacturer. GSR was easily found on wounds from days 1 and 2, however after a brief rainstorm, it appeared that the GSR may have been washed from the wounds. Weather plays an important role in the detection of GSR particles from gunshot wounds in tissue.

The Fe-Cr-Ni particles although interesting are not conclusive GSR evidence. If the particles were either found in conjunction with Sb, Ba, and Pb, they would be of greater significance, however since they lack the 'unique' elements, they are of little worth. Although it may be possible to determine if the particles were from the barrel of the gun the casings were not collected and investigation of the barrel composition is beyond the scope of this project.

4.5 Analysis of Tissue for GSR by ICPMS

4.5.1 ICPMS Calibration

Before the tissue digests were analyzed, the instrument was calibrated using standard solutions of ^{121}Sb, ^{138}Ba, and ^{208}Pb with concentrations of 0.5, 25, 250, 500, and 1000 ppb that were prepared in 2% nitric acid by serial dilution. In addition to the elements of interest, two internal standards were also used; indium (^{115}In) and bismuth (^{209}Bi). These elements were chosen as internal standards since their atomic masses are above and below the atomic masses of the target analytes, and they are not commonly encountered elements in high concentrations.

Internal and external standards were used in this study. The internal standards, ^{115}In and ^{209}Bi, served as a means to normalize the instrument response, and the external standards were used to quantify the concentration of target analyte based on the response. Figure 4.10 shows the resultant calibration curves generated for ^{121}Sb, ^{138}Ba, and ^{208}Pb. Each data point on the graph is the average of the detector response for three injections. The standard devation for each point was less than the data point itself so the error bars were omitted from the plot for clarity. The plot illustrates linearity for all three analytes in the range of 0 – 1000 ppb with r^2 values greater than or equal to 0.999 and intercepts at or near 0.

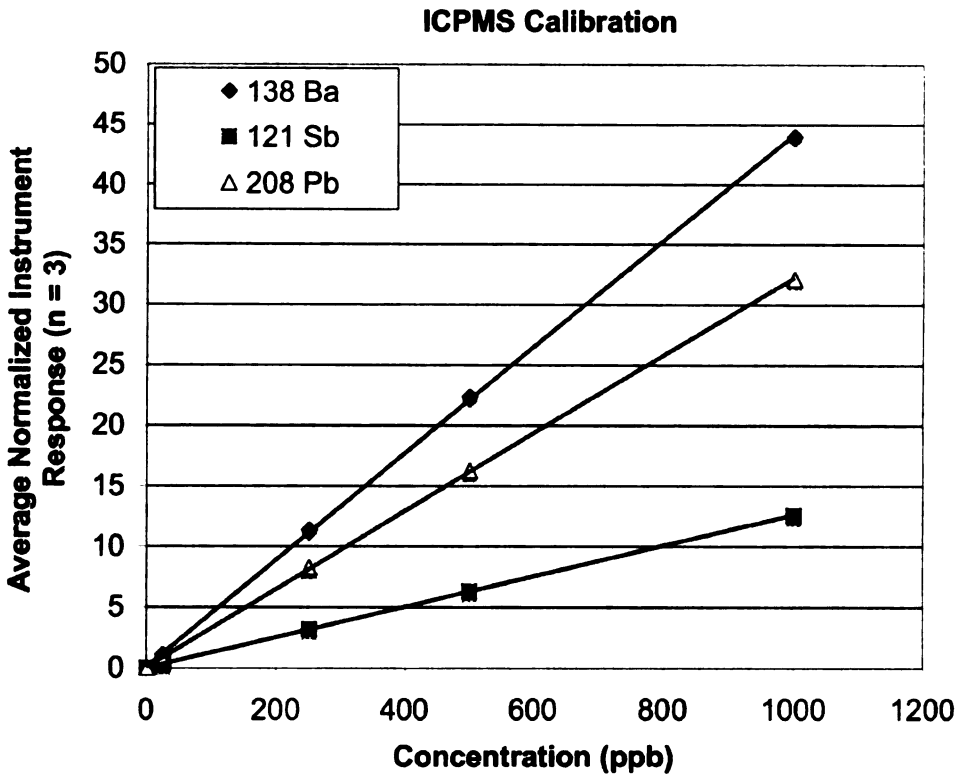

Figure 4.10 Calibration curves for the target analytes, ^{121}Sb, ^{138}Ba, and ^{208}Pb.

A 3σ detection limit was calculated from the calibration curve data as described by Koons.[44] The detection limit was determined by multiplying the standard deviation of the blank (concentration of 0 ppb) by three (3σ), then dividing by the sensitivity, which is the slope of the standard response curve for each element.[44] The detection limits for ^{121}Sb, ^{138}Ba, and ^{208}Pb were determined using the formula above and were 0.002, 0.033, and 0.009 ppb, respectively. These values are comparable to those Koons determined for the same analytes in GSR using ICPMS. Koons collected GSR from shooters hands with cotton swabs then digested the cotton tips in a vial of nitric acid. Koons' limits of detection for Sb and Pb were higher than those determined in this study by

approximately 1-2 orders of magnitude with values of 0.05 and 0.1 ppb, respectively. However, Koons reported a lower limit of detection for Ba (0.02 ppb) than the value reported herein (0.033).[44] The calibration curves illustrated that the ICPMS has a wide linear dynamic range and good sensitivity, which makes this instrument a valuable tool for trace elemental analysis.

4.5.2 ICPMS Precision

Ten separately prepared dilutions of the digest of a single gunshot wound sample were analyzed in order to evaluate the precision of the instrument and homogeneity of the sample. The data from these analyses can be seen in Table 4.3. The relative standard deviation (RSD) for the 10 injections was less than 3% for all three analytes, which is evidence attesting to the precision of the instrument and that the sample digests were homogeneous.

Table 4.3 ICPMS data for 10 individually prepared gunshot wound dilutions from day 3.

	Average (μg/g)	Relative Standard Deviation (RSD)
Antimony (^{121}Sb)	3.35	2.00%
Barium (^{138}Ba)	3.96	2.51%
Lead (^{208}Pb)	6.29	1.80%

4.5.3 ICPMS Analysis of Control Tissue Digests

Figure 4.11 shows example ICPMS spectra, with m/z along the x-axis and the relative percent intensity on the y-axis. The spectra for a gunshot wound and control tissue collected on day 3 illustrate the difference in the intensity of the

signal for the target analytes, ^{121}Sb and ^{138}Ba. The spectra are also provided to show that there are not many interfering peaks (i.e. low backgrounds) even though the analytes are in a complex matrix of digested tissue. The isotopes of Sb are present at m/z 121 and 123 and are observed in the wound tissue but not in the control.

The most abundant isotope of Ba is observed at m/z 138 in the gunshot tissue but not in the control. ^{138}Ba has a natural abundance of 72% and the next highest Ba isotope is ^{137}Ba with a natural abundance of 11%, approximately a 7:1 ratio between these peaks is expected and is seen in the spectrum peak intensities. ^{137}Ba should be the second most abundant isotope of Ba present in the spectrum. The peaks present at the other m/z corresponding to Ba isotopes (i.e 130, 132, 134, 135, 136) should therefore be of lesser intensity than ^{137}Ba if they truly corresponded to the isotopes. Although several other isotopes of Ba are observed in the spectra, they are likely interfering peaks from the matrix since they would not be present in such high concentrations naturally.

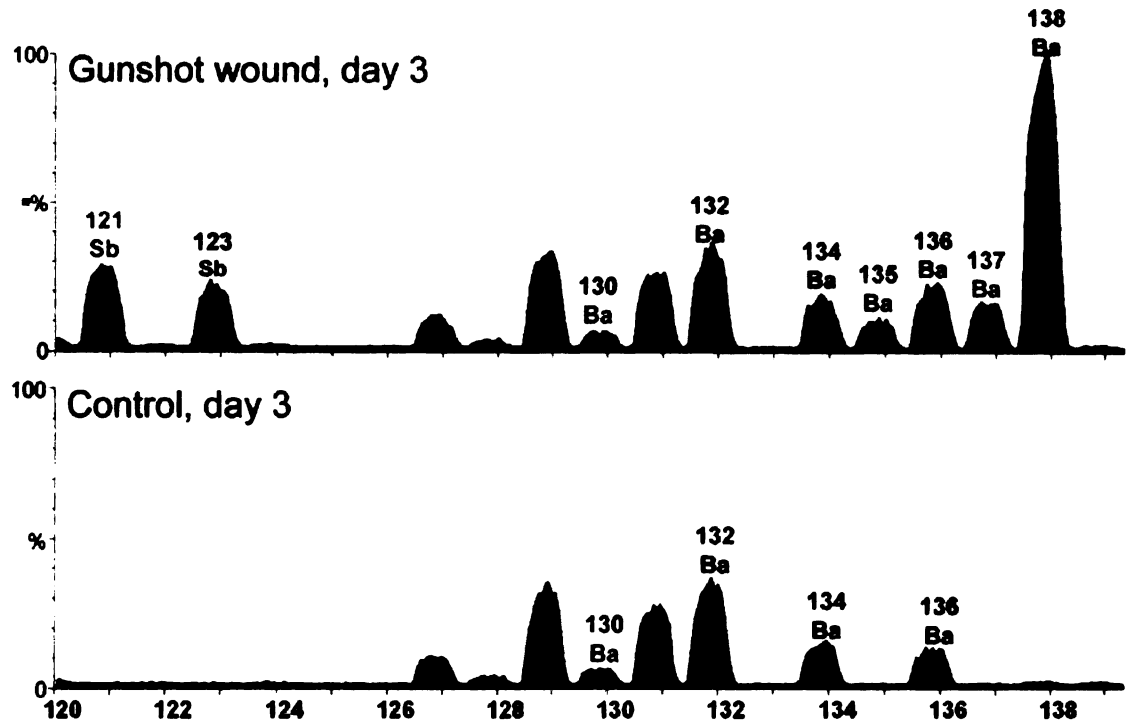

Figure 4.11 ICPMS spectra of the digests of a gunshot wound and control tissue from day 3. The spectra show the m/z range of 120 to 140 amu.

In Figure 4.12, the large peak appearing at m/z 209 is of ^{209}Bi, an element used as an internal standard throughout the study. ^{208}Pb is seen also in the wound tissue, but at much lesser intensity than the internal standard. No ^{208}Pb was observed in the control tissue.

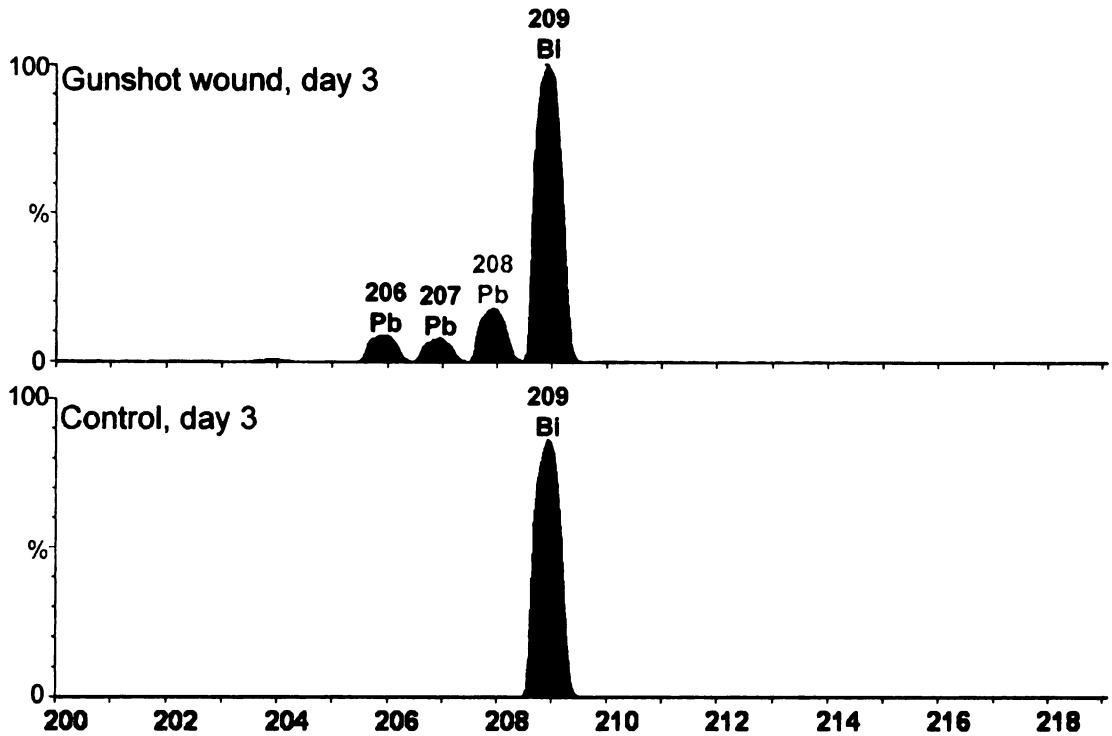

Figure 4.12 ICPMS spectra of the digests of a gunshot wound and control tissue from day 3. The spectra show the m/z range of 200 to 220 amu.

The control tissues collected from the seven consecutive days were analyzed. Figure 4.13 shows the plots of the concentrations of the target analytes versus the day of collection. A spike in the concentrations of ^{138}Ba and ^{208}Pb was observed, first occurring on day 5 and then fluctuating through day 7. The levels of ^{138}Ba increased from 0 μg/g on day 4 to 0.30 μg/g on day 5 followed by a decrease to 0.17 μg/g on day 6 and rising slightly on day 7 to reach 0.19 μg/g.

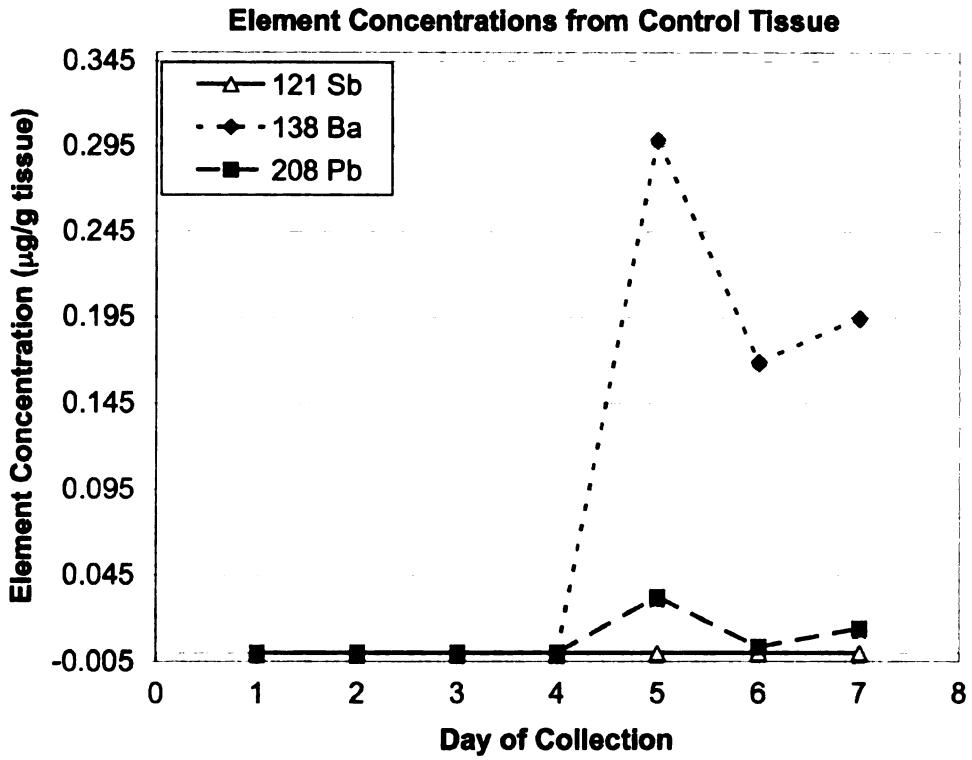

Figure 4.13 Plot of concentration of ^{121}Sb, ^{138}Ba, and ^{208}Pb versus the day of collection.

The level of ^{208}Pb increased from 0 µg/g on day 4 to 0.03 µg/g on day 5 followed by a decrease to 0.003 µg/g on day 6 and a rise to 0.01 µg/g on day 7. The levels of ^{208}Pb were much less than the ^{138}Ba during days 5, 6, and 7. The concentrations of ^{121}Sb remained at 0 µg/g for the entire 7-day sampling period. The observed spikes of ^{138}Ba and ^{208}Pb are of unknown origin although possible factors include; insects, rain, or other environmental factors such as fertilizer overspray since the entomology field is located adjacent to agricultural land. This observation provided evidence that GSR contamination was not the origin of the spiking since one would have expected to see elevations in all three elemental levels if that were the case. The differences in the levels of ^{121}Sb, ^{138}Ba, and

^{208}Pb were very small, their origin may be due to the different tissue samples collected on each day.

4.5.4 ICPMS Analysis of Gunshot Wound Tissue

Figure 4.14 is the concentration of ^{121}Sb, ^{138}Ba, and ^{208}Pb plotted versus the day of collection for the GSR tissue. The top plot is the full scale version of the graph and the plot below is the same plot except with the scale expanded to include only 0 – 1 μg/g. The plots show that with the passage of time, the concentration of elemental GSR decreased. The decreases from day 1 to day 7 were 9.19 μg/g to 0.15 μg/g for ^{121}Sb, from 30.67 μg/g to 0.06 μg/g for ^{138}Ba, and 26.71 μg/g to 0.10 μg/g for ^{208}Pb. The most significant decrease in concentration occurred for ^{121}Sb and ^{208}Pb between days 1 and 3. ^{138}Ba showed its greatest decrease between days 1 and 2, decreasing from 31 μg/g to 0.06 μg/g.

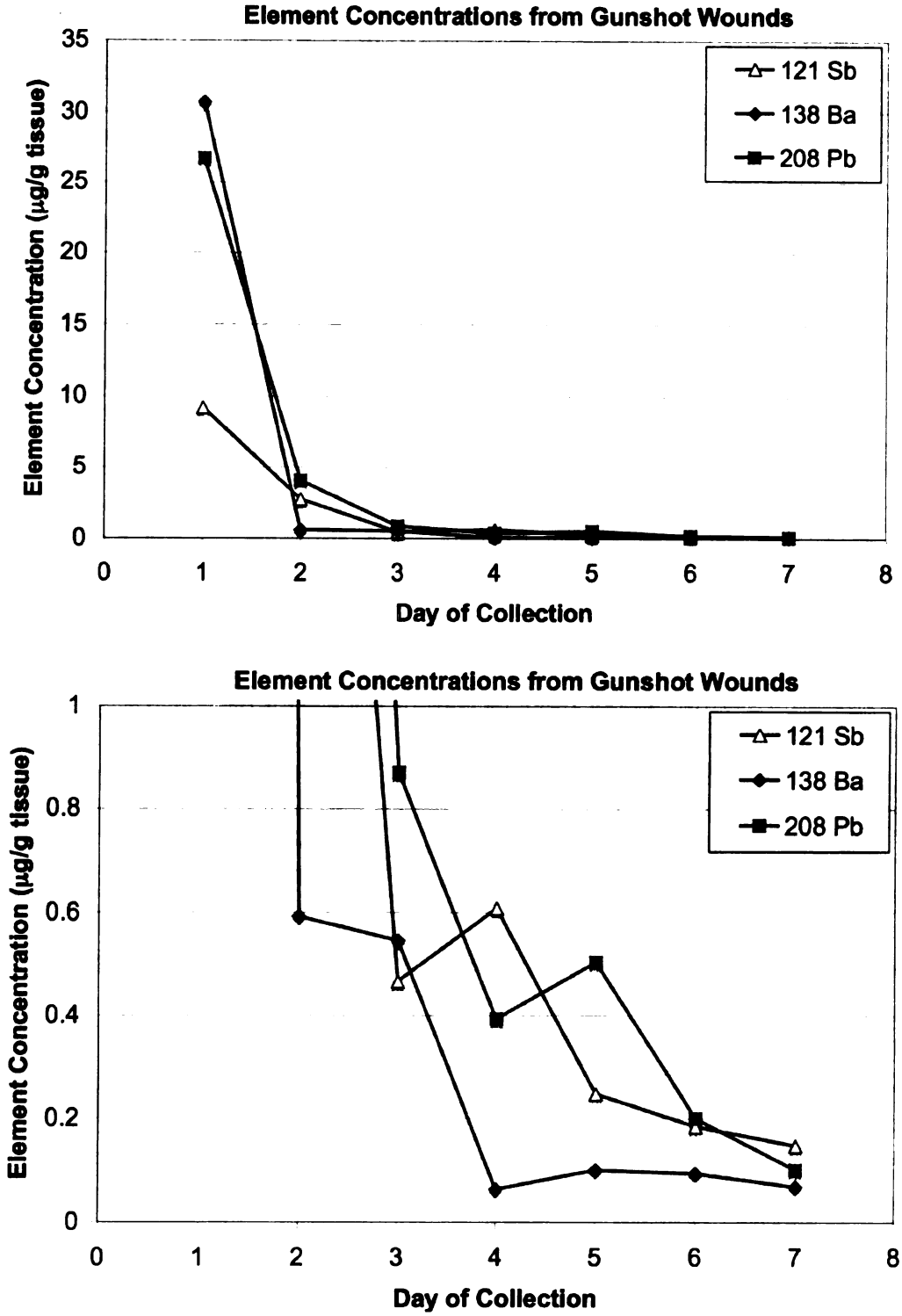

Figure 4.14 Plots of GSR concentration versus the day of collection. The upper plot is the full-scale version showing all of the data points and below is a magnified scale to show the values of GSR on later days of collection.

The drastic decrease in GSR within the first three days for all three elements is likely due, in part, to the weather. The rain on the evening of day 2 cannot account for all of the decrease of GSR, which was observed over the course of day 1 – 2, but it is believed to have some role in the decreases. It does not appear by the trends in Figure 4.14 plots that the hard rainfall on the night of day 5 had much of an effect on the concentrations of GSR on the wounds. The GSR on the tissue at these later stages of decomposition may have been embedded in the skin making the rain less effective at washing away the residues.

Although the overall trend for the GSR analytes was to decrease, spikes in the concentration of the analytes were seen on day 4 for ^{121}Sb, and day 5 for ^{138}Ba and ^{208}Pb. ^{121}Sb increased from 0.47 μg/g to 0.61 μg/g, ^{138}Ba increased from 0.06 μg/g to 0.10 μg/g, and ^{208}Pb increased from 0.39 μg/g to 0.50 μg/g. The increases that were observed were all less than 150 ng/g of each respective analyte and hence, were considered to be of little concern. The small increases could be due to differences in the weathering and/or decomposition of each particular wound. The fact that each sample was a different, separately collected tissue from a different area of the animal may be enough to account for these small variations of element concentrations.

4.5.5 Concentrations of the Analytes in Tissue Digests

Table 4.4 contains the concentrations of each analyte in the gunshot wounds and control tissues analyzed for each day. For the control tissue, Sb

remains below the instrument's limit of detection throughout the 7-day sampling period. Pb was below the LOD until day 5 when the concentration increased to 30 ng/g. The levels of Pb were very low during days 5, 6, and 7 and are less than the concentrations observed in the gunshot wounds.

The elevation of ^{138}Ba in the gunshot wound tissue that occurred from days 4 to 5 was also seen in the control tissue, although at much greater levels. The gunshot wound tissue ^{138}Ba increased very slightly from 0.06 μg/g to 0.10 μg/g, a total of 40 ng, whereas the control tissue increased from 0 μg/g to 0.30 μg/g, a total of 300 ng. Although the increases occur over the same time period, it cannot be concluded that they are related due to the discrepancy in the magnitude of elevation between them. Had the increases been more systematic, it may have been possible to relate the increases to some common source.

Table 4.4 ICPMS data for the gunshot wounds and control tissue collected during the course of the 7-day sampling period.

Tissue	Elements	Day 1	Day 2	Day 3	Day 4	Day 5	Day 6	Day 7
Control (μg/g)	Sb	-	-	-	-	-	-	-
	Ba	-	-	-	-	0.30	0.17	0.19
	Pb	-	-	-	-	0.03	0.003	0.01
Gunshot Wound (μg/g)	Sb	9.19	2.75	0.47	0.61	0.25	0.18	0.15
	Ba	30.7	0.60	0.55	0.06	0.10	0.09	0.07
	Pb	26.7	4.07	0.87	0.39	0.50	0.20	0.10

4.5.6 ICPMS Analysis of Procedural Blanks

The procedural blanks that were analyzed along with the control and GSR samples did not contain any significant levels of the target analytes. The

concentrations contained in the procedural blanks were 0.5 ± 1.0, 0.1 ± 0.2, and 0.2 ± 0.5 ppb for ^{121}Sb, ^{138}Ba, and ^{208}Pb respectively. These concentrations were much lower than any of the levels encountered in the GSR samples which for day 7, the lowest values, were 29 ppb for ^{121}Sb, 13 ppb for ^{138}Ba, and 20 ppb for ^{208}Pb. Thus, it can be concluded that the levels of GSR analytes within the tissue were not significantly affected by the solutions or preparation. Hence, there was no significant contamination contributing to the GSR, i.e. the levels observed were truly GSR.

4.6 Summary of ICPMS Results

The results presented in this chapter are the first known application of ICPMS for analysis of GSR directly from decomposing tissue. There have been several papers that have discussed the use of ICPMS for the trace metal analysis of GSR from cotton-tipped swabs, cotton paper, and blowfly larvae as discussed in Chapter 2 but, according to a recent survey of literature, never for tissue containing GSR. The most important outcome of this study is that the results were successful. Preliminary findings illustrated that ICPMS does have the capabilities to easily detect GSR through the complex digested tissue matrix. The ICPMS used in these studies had low detection limits, two of which, ^{121}Sb and ^{208}Pb, were lower than previously reported values.[44] The precision of the ICPMS was demonstrated with the gunshot wound samples. A tissue digest was prepared for 10 separate analyses and a RSD of less than 3% for the 10 sample injections for each element were obtained.

GSR was determined in gunshot wounds throughout the period of 7 days despite unfavorable weather conditions. The concentration of the initial digest solution from the gunshot wound of day 7 was 29, 13, and 20 ppb for ^{121}Sb, ^{138}Ba, and ^{208}Pb respectively, all of which were greater than the detection limits of the instrument. The solutions analyzed, however, were diluted from the initial tissue digest by a factor of 43.3. If no GSR was detected during the later stages of the experiment, then a less dilute sample could easily be prepared for analysis.

The levels that were detected during the later stages (days 5-7) of decomposition were very low ranging from 0.61 μg/g to 0.15 μg/g for ^{121}Sb, 0.06 μg/g to 0.10 μg/g for ^{138}Ba, and from 0.39 μg/g to 0.10 μg/g for ^{208}Pb in tissue. The control tissues from the 7-day period had undetectable levels of ^{121}Sb, ^{138}Ba, and ^{208}Pb for the first four days. On day 5, there was a spike in the levels of ^{208}Pb and ^{138}Ba, and they remained at elevated fluctuating levels for the remainder of the study. Currently, there is no known explanation for this elevation in analyte concentrations. The ^{121}Sb, however did not become elevated throughout the course of this study. Additional control tissue would need to be analyzed to determine the origin of the ^{138}Ba and ^{208}Pb levels. The ICPMS has been shown as a technique with great potential for analysis of GSR even at trace levels from complex sources.

Chapter 5

Chapter 5

Conclusions and Further Work

5.1 Conclusions

This preliminary project was designed to lay the foundation for future work in GSR research. The research addresses a particular issue within forensic analysis; that is the identification or detection of a gunshot wound or gunshot residue on decomposing tissue. The project aimed to detect and analyze GSR from decomposing tissue within two different domains; morphology and elemental composition of individual particles with SEM/EDS and also elemental composition of bulk samples with ICPMS. Both avenues of this research project had successful results.

Air-drying and freeze-drying gunshot wounds for direct SEM/EDS analysis of GSR was attempted. SEM/EDS was found to be of limited use for GSR analysis directly from tissue samples. Tissues imaged under the SEM were easily damaged by the electron beam and were of poor quality, making the location and analysis of GSR particles difficult. GSR was also obscured by the large amount of hair and debris on the samples. The preparation of samples was also labor intensive and time-consuming, beginning with the removal of adipose tissue with a scalpel to that of drying the sample by either of the methods. Both air- and freeze-drying required greater than 48 hours.

Tape lifting was determined to be the most effective method of sample preparation for GSR analysis in terms of both time and ease of preparation. Tape lifts from the gunshot wounds and control tissues were analyzed by SEM/EDS and GSR was found to be dense on wounds from days 1 and 2. The GSR particles that were located and analyzed had a slightly deformed spherical shape with a diameter ranging from 0.5 – 1 μm and had elemental compositions of Sb, Ba, and Pb. On days 3-7, no distinct GSR containing significant levels of Sb, Ba, and Pb were located. However, on days 5 and 6, spherical particles with no observed deformation were found. The particles were analyzed by EDS and had an elemental composition of Fe-Cr-Ni, which is consistent with stainless steel possibly from the barrel of the gun.

For ICPMS, the samples were fully digested in nitric acid, diluted, and analyzed by ICPMS. The ICPMS was shown to have a linear response between 0 and 1000 ppb for ^{121}Sb, ^{138}Ba, and ^{208}Pb. Precision of the instrument was demonstrated with less than a 3% RSD for all three elements over the course of 10 sequential replicate injections. The limits of detection for the target elements were 0.002 ppb for Sb, 0.033 ppb for Ba, and 0.009 ppb for Pb. The limits of detection for Sb and Pb were 1-2 orders of magnitude lower than those reported for GSR detection by Koons.[44]

GSR was detected in the gunshot wound tissues collected throughout the 7-day period and was determined as the elemental components, ^{121}Sb, ^{138}Ba, and ^{208}Pb. ^{121}Sb and ^{208}Pb showed a significant decrease in concentration over the course of days 1-3; ^{121}Sb dropped from an initial concentration of 9.2 μg/g of

tissue to 0.5 μg/g and ^{208}Pb dropped from an initial concentration of 26.7 μg/g to 0.9 μg/g. The GSR levels found in the gunshot wounds, even at the end of the 7-day period, were well above the limits of detection for each of the elements. A more abrupt decrease in concentration was observed for ^{138}Ba. Over the course of days 1-2, the concentration of ^{138}Ba dropped from 30.7 μg/g to 0.7 μg/g.

Control tissues were also analyzed by ICPMS and for days 1-4, none of the GSR elements were detected. On day 5, there was a spike in the concentrations of ^{138}Ba and ^{208}Pb in the control tissues. ^{138}Ba increased to 0.3 μg/g and ^{208}Pb increased to 0.03 μg/g, their concentrations then fluctuated for the following 2 days. There was no explanation for these observed increases at the current time.

Lastly, the weather was seen to have an effect on the levels of GSR present on the wounds by SEM/EDS. SEM/EDS analysis showed that after the first rainstorm, during the night of day 2, there were no detectable GSR particles. ICPMS showed significant decreases in GSR but not anything directly attributable to the weather experienced throughout the course of the week. The rapid decrease of GSR observed by SEM/EDS between days 2 and 3 was also seen by ICPMS in the form of an abrupt decrease in the GSR elements. Although no GSR was found by SEM/EDS after day 2, ICPMS was able to determine the presence of GSR throughout the entire 7-day sampling period.

5.2 Further Work

There are many opportunities within the framework of this research for new projects. The first and most obvious project would be expanding the ICPMS analyses for a larger sample size to allow for statistical conclusions to be drawn. Expanding the sampling period would also be interesting since after 7 days, GSR was still determined in gunshot wounds collected throughout this study. The tissue digests analyzed in this study were dilute and the analytes could still be detected, analysis of undiluted samples should allow for the extension of the sampling period. Another study assessing the effect of GSR deposition when the barrel of the firearm is not cleaned between shots could be completed. During this study, the firearm was cleaned between shots. Hence, a comparison of the GSR concentrations determined herein with the concentrations from a handgun that was not cleaned could be made. The study would determine if GSR levels increase linearly with each shot and whether the firing order could be determined by the relative levels of GSR and/or if one or more elements increases more so than another.

Comparison of different firearms and ammunition as well as varying the distance of firing would also be extremely interesting studies. The use of different firearms and ammunition would provide an assessment of whether trace elements originating from the gun barrel, cartridge, or other components could be detected, possibly allowing for firearm and ammunition differentiation or elimination in a crime. Varying the distance from which the firearm was discharged from the target would provide elaboration of Santos' work with ICPMS

and GSR.[5] Santos' study marked the start of the development of a statistical GSR versus distance model, but certainly not the end. In addition to Sb, Ba, and Pb, other trace elements present in the GSR could also be determined, such as Al, Zn, Si, or others described in literature.[7, 27] The use of trace elements could provide another dimension to GSR analysis, such as determining the manufacturer of the ammunition or even the propellant type or whether the bullet was jacketed or not. All of these projects would highlight a particular area in GSR analysis, which up until this point, had not been researched thoroughly.

The SEM/EDS analysis produced similar conclusions to previous publications in which tape lifting was demonstrated as a superior method of sample collection for this type of analysis.[22] This research has demonstrated that ICPMS is a valuable tool for GSR analysis, it is sensitive, has a wide linear dynamic range and good response stability. This study is the first known application of ICPMS for the determination of GSR in decomposing tissue. The findings from this project provide a foundation from which improvements can be made.

1. Justice, U. S. D. o. Bureau of Justice Statistics, Firearms and Crime Statistics. http://www.ojp.usdoj.gov/bjs/guns.htm (March 07),

2. Violence, T. C. t. S. G. CSGV Briefing Book. (March 17),

3. Collins, K. A.; Lantz, P. E., Interpretation of Fatal, Multiple and Exiting Gunshot Wounds by Trauma Specialists. *Journal of Forensic Sciences* **1994,** 39, (1), 94-99.

4. Denton, J. S.; Segovia, A.; Filkins, J. A., Practical Pathology of Gunshot Wounds. *Archives of Pathology Laboratory Medicine* **2006,** 130, 1283-1289.

5. Santos, A. S.; Magalhaes, T.; Nuno Vieira, D.; Almeida, A. A.; Sousa, A. V., Firing Distance Estimation Through the Analysis of the Gunshot Residue Deposit Pattern Around the Bullet Entrance Hole by ICPMS. *The American Journal of Forensic Medicine and Pathology* **2007,** 28, (1), 24-30.

6. Hussain, G.; Rees, G. J., Combustion of Black Powder. Part 1. *Propellants, Explosives, Pyrotechnics* **1990,** 15, (2), 43-47.

7. Meng, H.; Caddy, B., Gunshot Residue Analysis. *Journal of Forensic Sciences* **1997,** 42, (4), 553-570.

8. Romolo, F. S.; Margot, P., Identification of Gunshot Residue: A Critical Review. *Forensic Science International* **2000,** 119, 195-211.

9. Basu, S., Formation of GSR. *Journal of Forensic Sciences* **1982,** 27, (1), 72-91.

10. Di Maio, V. J. M., *Gunshot Wounds: Practical Aspects of Firearms, Ballistics, and Forensic Techniques.* CRC Press: Boca Raton, 1993; p 331.

11. Burrard, G., *The Identification of Firearms and Forensic Ballistics.* 2nd ed.; Wolfe Publishing Company: London, 1951; p 217.

12. Doyle, J. S. Gunshot Residue. http://www.firearmsID.com/A_DistanceGSR.htm (March 07),

13. Lebiedzik, J.; Johnson, D. L., Handguns and Ammunitions Indicators Extracted from the GSR Analysis. *Journal of Forensic Sciences* **2002,** 47, (3), 483-493.

14. Wolten, G. M.; Nesbitt, R. S., On the Mechanism of GSR Particle Formation. *Journal of Forensic Sciences* **1980,** 25, (3), 533-545.

15. Torre, C.; Mattutino, G.; Vasino, V.; Robino, C., Brake Linings: A Source of Non-GSR Particles Containing Lead, Barium and Antimony. *Journal of Forensic Sciences* **2002,** 47, (3), 494-504.

16. Zeichner, A., Recent Developments in Methods of Chemical Analysis in Investigations of Firearm-related Events. *Analytical and Bioanalytical Chemistry* **2003,** 376, 1178-1191.

17. Morales, E. B.; Revila Vazquez, A. L., Simultaneous Determination of Inorganic and Organic GSR by CE. *Journal of Chromatography A* **2004,** 1061, 225-233.

18. Tschirhart, D. L.; Noguchi, T. T.; Klatt, E. C., A Simple Hitochemical Technique for the Identification of GSR. *Journal of Forensic Sciences* **1991,** 36, (2), 543-547.

19. D'Uffizi, M.; Falso, G.; Ingo, G. M.; Padeletti, G., Microchemical and Micromorphological Features of GSR Observed by Combined Use of AFM, SA-XPS, and SEM/EDS. *Surface and Interface Analysis* **2002,** 34, 502-506.

20. Woolever, C. A.; Starkey, D. E.; Dewald, H. D., DP-ASV of Lead and Antimony in GSR. *Forensic Science International* **1999,** 102, 45-50.

21. Stein, K. M.; Bahner, M. L.; Merkel, J.; Ain, S., Detection of GSR in Routine CTs. *International Journal of Legal Medicine* **2000,** 114, 15-18.

22. DeGaetano, D.; Siegel, J. A.; Klomparens, K. L., A Comparison of Three Techniques for Sampling and Analysis of GSR by SEM/EDX Analysis. *Journal of Forensic Sciences* **1992,** 37, (1), 281-300.

23. Zeichner, A.; Ehrlich, S.; Shoshani, E.; Halicz, L., Application of Lead Isotope Analysis in Shooting Incident Investigations. *Forensic Science International* **2005**.

24. Ravreby, M., Analysis of Long-Range Bullet Entrance Holes by AAS with SEM. *Journal of Forensic Sciences* **1982,** 27, (1), 92-112.

25. Ruch, R. R.; Buchanan, J. D.; Guinn, V. P.; Bellanca, S. C.; Pinker, R. H., NAA in Scientific Crime Detection. *Journal of Forensic Sciences* **1964,** 9, 119-132.

26. Koons, R. D.; Havekost, D. G.; Peters, C. A., Analysis of GSR Primer Residue Using FAAS: A Reexamination of Extractions and Instrument Procedures. *Journal of Forensic Sciences* **1987,** 32, (4), 846-865.

27. Romolo, F. S.; Margot, P., Identification of Gunshot Residue: A Critical Review. *Forensic Science International* **2001,** 119, 195-211.

28. JEOL, L. SEM Products Info. http://www.jeol.com/Default.aspx?tabid=102 (March 21),

29. Tillman, W. L., Automated GSR Particle Search and Characterization. *Journal of Forensic Sciences* **1987,** 32, 62-71.

30. White, R. S.; Qwens, A. D., Automation of GSR Detection and Analysis by SEM/EDS. *Journal of Forensic Sciences* **1987,** 32, 1595-1603.

31. Roeterdink, E. M.; Dadour, I. R.; Watling, R. J., Extraction of GSR from the Larvae of the Forensically Important Blowfly. *International Journal of Legal Medicine* **2004,** 118, 63-70.

32. Breton, B. C., The Early History and Development of the SEM. In Cambridge, 2006; Vol. 2007.

33. Flegler, S. L.; Heckman, J. W.; Klomparens, K. L., *Scanning and Transmission Electron Microscopy: An Introduction*. Oxford University Press: New York, 1993; p 225.

34. American Society for Testing and Materials, I., Standard Guide for GSR Analysis by SEM/EDS. In *ASTM E1588-95*, ASTM: West Conshohocken, 2000; Vol. 14.02, pp 657-659.

35. Boehm, A., Application of the SEM in Forensic Medicine. *Scanning Electron Microscopy* **1971,** 62, 553-560.

36. Kage, S.; Kudo, K.; Kaizoji, A.; Ryumoto, J.; Ikeda, H.; Ikeda, N., A Simple Method for Detection of GSR Particles from Hands, Hair, Face ad Clothing Using SEM/WDX. *Journal of Forensic Sciences* **2001,** 46, (4), 830-834.

37. Beauchemin, D., ICPMS. *Analytical Chemistry* **2006,** J Pages, J.

38. McCurdy, E.; Potter, D., ICPMS. In *Atomic Spectroscopy in Elemental Analysis*, Cullen, M., Ed. Blackwell Publishing Ltd.: Boca Raton, 2004.

39. Skoog, D. A.; Holler, F. J.; Nieman, T. A., *Principles of Instrumental Analysis*. 5 ed.; Books/Cole Thomson Learning: Crawfordsville, 1998.

40. Olesik, J. W., Elemental Analysis Using ICP-OES and ICP/MS. *Analytical Chemistry* **1991,** 63, (1), 12A-21A.

41. Meyer, G. A., ICP. *Analytical Chemistry* **1987,** 59, (23), 1345A-1354A.

42. Ebdon, L.; Evans, E. H.; Fisher, A.; Hill, S. J., *Analytical Atomic Spectrometry*. John Wiley and Sons, Ltd.: West Sussex, 1998.

43. Cottingham, K., *Analytical Chemistry* **2004**, 35A-38A.

44. Koons, R. D., Analysis of Gunshot Primer Residue Collection Swabs by ICPMS. *Journal of Forensic Sciences* **1998,** 43, (4), 748-754.

45. Reis, E. L.; Sousa Sarkis, J. E.; Neto, O. N.; Rodriguez, C.; Kakazu, M. H.; Viebig, S., A New Method for Collection and Identification of GSR from the Hands of Shooters. *Journal of Forensic Sciences* **2003,** 48, (6), 1269-1274.

46. Souza Sarkis, J. E.; Neto, O. N.; Viebig, S.; Durrant, S. F., Measurements of GSR by Sector Field ICPMS - Further Studies with Pistols. *Forensic Science International* **2007,** In press.

47. Singer, R. L.; Davis, D.; Houck, M., A Survey of GSR Analysis. *Journal of Forensic Sciences* **1996,** 41, (2), 195-198.

48. Haag, M.; Wolberg, G., Scientific Examination and Comparison of Skin Simulants for Distance Determinations. *The Journal of the Association of Firearm and Toolmark Examiners* **2000,** 32, (2), 136-142.

49. Megyesi, M. The Effects of Temperature on the Decomposition Rate of Human Remains. University of Indianapolis, Indianapolis, 2001.

50. Archer, M., Rainfall and temperature effects on the decomposition rate of exposed neonatal remains. *Science and Justice: Journal of the Forensic Science Society* **2004,** 44, (1), 35-41.

51. Miyauchi, H.; Kumihashi, M.; Shibayama, T., The Contribution of Trace Elements from Smokeless Powder to Post Firing Residues. *Journal of Forensic Sciences* **1998,** 43, 90-96.